UFL/COEL-93/006

VIDEO MONITORING TECHNIQUES IN THE COASTAL ENVIRONMENT

by

Timothy P. Mason

Thesis

1993

VIDEO MONITORING TECHNIQUES IN THE COASTAL ENVIRONMENT

By

TIMOTHY P. MASON

A THESIS PRESENTED TO THE GRADUATE SCHOOL
OF THE UNIVERSITY OF FLORIDA IN PARTIAL FULFILLMENT
OF THE REQUIREMENTS FOR THE DEGREE OF
MASTER OF ENGINEERING

UNIVERSITY OF FLORIDA

1993

ACKNOWLEDGMENTS

I wish to express a great deal of thanks to my advisor and supervisory committee chairman, Dr. Daniel M. Hanes, for his support and guidance during my stay at the University of Florida. I would also like to thank the members of my supervisory committee, Dr. Robert G. Dean and Dr. Robert J. Thieke. Also many thanks go to Dr. Rusty Erdman, without whom this endeavor into the video realm would not have been possible.

I would also like to thank the field crew at the Coastal Engineering Laboratory, Mark Sutherland and Vic Adams, and fellow students, Phil Dompe and Chris Jette, for assistance during field deployments and surveys. I am greatly indebted to the coastal secretarial staff, Becky, Sandra, Cynthia, and Lucy, for their crucial clerical support. Thanks also go to Helen for the goodies that keep the coastals working hard. I need to thank my parents Faye and Richard Badman for providing me the mind, body, and support to exceed in all my endeavors. I am also indebted to Paula and Bob Kelly for much-needed summer employment, financial assistance, and many great times. Mr. Robert Janssen, wherever he may be, is responsible making my desire to ride waves a reality and an obsession.

Miscellaneous kudos go to my friends who kept me entertained during this work: Quazi, Paul (the man), Dagwood, Joe, and Eric. Thanks for entertainment and sanity checks go to Dominical and Tamarindo, Reggie and Mike, Rob (for the awesome boards and adventures), Market Street Pub and St. George's Tavern, Squeeze, the Mons and the Diamond Club, the greatest drummers of the world, rock and roll, Beavis and Butt-head (that would be cool), Dos Equis, Imperial, Fosters Lager, and (most importantly) waves.

TABLE OF CONTENTS

LIST OF FIGURES

LIST OF TABLES

LIST OF SYMBOLS

f_c	focal length
ϕ	camera azimuth angle
H	exposure station elevation
H_s	significant wave height
NTU	turbidity, in Nephelometric Turbidity Units
P	ground location coordinate
p	image location coordinate
s	camera swing angle
τ	camera tilt angle
θ	horizon tilt angle
Θ	peak wave direction
U	cross shore current velocity
V	longshore current velocity
Z_p	ground point elevation

Abstract of Thesis Presented to the Graduate School
of the University of Florida in Partial Fulfillment of the
Requirements for the Degree of Master of Engineering

VIDEO MONITORING TECHNIQUES IN THE
COASTAL ENVIRONMENT
By

Timothy P. Mason

December 1993

Chairman: Daniel M. Hanes
Major Department: Coastal and Oceanographic Engineering

The field of coastal engineering has primarily utilized traditional measurement techniques such as boat surveys and beach profiles. Aerial photography has played a major role in the mapping of coastlines and ocean currents. More recent technology has provided the ability to make field measurements with precision electronic instrumentation, but the problem of making large-scale measurements within economic bounds remains. The video revolution and, in particular, desktop video has greatly enhanced the ability of scientists and engineers to visualize events over greater periods of time and larger scales than ever before.

The uses of video, benefits, shortcomings, and future expectations are presented as applicable to the field of coastal engineering. This feasibility study incorporates some applications which have previously been explored, as well as others which result from two unique video data sets that were collected between 1991 and the present.

Using a rectification procedure and image processing system, video estimates of general length scales and shoreline position have been found to be within 5% of survey data. Accuracy depends on the camera and camera set up, type of image used, view

geometry, and subsequent image manipulations. Nearshore sand bar dimensions and location are observed using a time averaging technique. Beach fill progress during a beach renourishment is monitored by measuring changes in shoreline location. Rip currents and other turbidity structures, both natural and man-induced, are observed and mapped over time. Although the forcing of such turbidity events is not fully explained, the influence of waves and coastal advective currents is shown. The turbidity patterns tend to form after periods of increased wave activity or during beach renourishment. Cross shore and longshore velocities of observed turbidity plumes are similar to in-situ currents measured during the Hollywood Beach renourishment of summer 1991. Turbidity plumes mapped at Hollywood Beach may extend offshore over 3 times the width of the surf zone and have typical wavelengths around 5 times the width of the surf zone.

Video monitoring has proven to be a useful and cost-effective way to perform traditional observations and also to document events that would not normally be possible to record with standard instrumentation in the coastal environment. The nature of the typical oblique views and digital imagery places some limitations on the accuracy of the applications, but the large spatial scale and flexible temporal scale make video monitoring an attractive option.

CHAPTER 1
INTRODUCTION

The old adage "a picture is worth a thousand words" is quite appropriate to summarize the concept of video monitoring. The field of coastal engineering, still in relative infancy, has traditionally utilized visual measurements coupled with standard measurement techniques. These techniques include surveys with differential levelling, hydrographic surveys with transducers, and wave staffs, to name a few. Aerial photography and acoustic instrumentation have also contributed to a more comprehensive understanding of coastal processes.

The use of video monitoring, particularly in the coastal environment, has resulted from several circumstances. The video revolution and recent advances in desktop video have put video equipment within the reach of consumers. People are familiar with video, which produces a quality image that can convey information much faster than the written word. A video image (for example, of a segment of the coast) transmits much information about the given scene, over a large spatial scale. Weather, sea conditions, beach traffic, ship traffic, and coastal features are some of the obvious pieces of information which can be visually assessed from video images. With time lapse video, the long term events and processes can be studied.

1.1 Objectives, Scope, Tasks

The primary purpose of this paper is to introduce the concept of video monitoring to the coastal scientist and engineer. Few investigators have used video for coastal

research applications over the last decade, so a literature review is provided in Section 1.3. The developments in video monitoring techniques are presented. The basic principles of images and their analysis are discussed. The video monitoring system hardware and software, installation, and uses are presented.

Techniques of image interpretation for coastal applications are discussed, but the highest emphasis is placed on the feasibility of using video for coastal observations. From our preliminary (and prototype) systems and data collections, the "dos and don'ts" of video monitoring have become clear. This report is an introduction to video monitoring, to present the benefits and drawbacks of such systems, and to inspire interest in others to pursue the suggested techniques in greater detail.

1.2 Upcoming Chapters

Section 1.3 contains a short literature review of prominent work that has been done with video monitoring (and related subjects) over the last two decades. Important entries are merely summarized. Interested readers are strongly suggested to consult the references provided for details.

Chapter 2 contains the data collection information from the past two years of research. The video monitoring system and the field deployments are described. Chapter 3 presents the basics of image analysis. An introduction to digital image concepts, photogrammetry, image rectification and other methods are discussed. Chapter 4 contains the results and discussion of the gathered and analyzed data. Some areas considered have been previously covered, while others are unique to this research. Chapter 5 contains conclusions and a summary of this study, as well as recommendations for current and future video monitoring endeavors. Equipment, vendors, and computer program listings are presented in the appendices.

1.3 Literature Review

As far back as the 1940s, coastal engineers were beginning to use photography for qualitative assessment of coastal features. Aerial photographs and satellite images have been integral in the mapping of the world coastlines and other large scale features of the oceans. Presented herein are several of the papers from the past two decades which introduced video monitoring and brought it to the level of today. It is noted that the field is limited; there is not much reference literature available.

Prior to the video revolution, which can be dated back to the early 1980s, the emphasis was placed on the use of terrestrial photographs for interpretation. Photogrammetric techniques for interpretation of oblique photographs have been well known for many years. Loomer and Wolf (1974) used land-based cameras to map water surface velocities on Lake Michigan. A camera was set up on a bluff at 30 m above the lake water level. Oblique photographs were taken of drogues which were deployed on the lake to map outfall currents. Using traditional photogrammetric techniques, Loomer and Wolf determined that errors in measurements increase with distance from the camera. Errors in velocity estimates were up to 10% for drogues that were 213 m from the camera.

In 1976, Maresca and Seibel used a similar technique to measure breaking waves and currents in the nearshore region. Two techniques were investigated: single oblique photos and stereo pairs (the concept of stereo image analysis extends beyond the scope of this paper and will not be included). Several important points were made. Maresca and Seibel pointed out that if the tilt of the apparent horizon is less than 1°, then no corrective measures need to be taken to account for a slightly tilted horizon (which would introduce roll effects in the images). Using a 35 mm camera on a voice timer, snapshots were taken and analyzed to determine breaker location, nearshore wavelength, runup, and ice ridge location. With the camera mounted on an 8 m bluff, the maximum useful range was found to be 250 m. Accuracies of measured distances were better than 1% horizontally

and 10% vertically. Breaker height estimates were found to have accuracies around 10%, but the difficulty was in determining the true location of the trough of the waves from the photographs. Some current mapping was also investigated with the use of dye packs placed in the surf zone. For single oblique shots, Maresca and Seibel note that no reference stakes are required for image calibration if the horizon, camera elevation, and focal length are known.

The most prolific group on the subject of video monitoring for coastal applications is under Dr. Rob Holman at Oregon State University. Holman and Guza (1984) used time-lapse photography to measure run-up. Photo measurements were "intercalibrated" with standard dual-resistance wire sensors. At this early stage, the photos (slides) were projected on a screen and digitized manually. This subjectivity and tedious nature of the manual digitization gave way to further improvements, but the compared results were quite accurate (a small difference in set-up measurements, but up to 83% difference in swash variance). The main advantage of the photographic technique was the ability to make measurements in storm conditions, when coastal engineering interests peak.

Lippmann and Holman (1987) developed a technique for modeling and measuring 3D morphology of submerged features during the DUCK'85 field experiment. 35 mm cameras were set up on a 14 m tower, but 10 minute time exposures were taken instead of single snapshots. The time exposure essentially averages over the modulations of the incoming, random waves. Again, photographs were analyzed with the subjective digitization process. A small data set was used to test the model which was based on the preferential breaking of incoming waves over shallower areas and sand bars. This technique, like Maresca and Seibel, was operational during all types of conditions (except darkness) and covered a much larger spatial area than practical with traditional survey techniques. Lippmann and Holman's initial tests showed that errors in measurements made with the photographic technique are within 2% of the distance from the camera and

up to 15% on bars with an incoming tide. No initial effect on the time exposure technique due to wave size was initially seen.

Lippmann and Holman (1989) presented results from the SUPERDUCK experiment (1986). They improved upon their earlier concept in several ways. The previous model was updated and based on a random wave model, with the assumption that light intensity (and hence, image intensity) is proportional to the energy dissipated by breaking waves. The dissipation model was found to work best for waves that just break over the bar and at lower tides.

Of significant importance was the medium transition from standard photography to video. A black and white video camera was mounted on a 40 m tower and recorded 20 minute records each hour. A computer-based image processing system was introduced to simulate a time exposure by time averaging successive frames. The image processing system was also used to generate intensity plots for selected cross shore and long shore profiles. The intensity plots were compared with substantial survey data which was collected during SUPERDUCK. Also presented were the photogrammetric equations of geometrical transformation for measurement from oblique images and rectification.

The results of analysis showed that for a camera elevation of 40 m and tilt of 85°, the worst-case error in measurements was less than 5% of the distance to the camera. When the wave field became saturated (during large wave conditions), it was observed that the location of the bar crest was consistently displaced seaward with up to a 35% error in determination of the crest location. Accurate bar crest location was also affected by high onshore winds and persistent foam which remains shoreward of the bar area after waves break.

To remove the "noisy" signal of the foam, Lippmann and Holman employed a differencing technique. This technique is basically the reverse process of time averaging. Instead of adding frames, successive frames (0.5 to 1.0 second apart) were subtracted. In the resulting image, areas of small change in contrast exhibit no difference. Breaking

areas exhibit large intensity changes over time, therefore large difference signals. The differencing method improved the accuracy of the bar crest location determination.

General conclusions of Lippmann and Holman (1989) are as follows. First, the time averaging technique presents a generally good method of determining submerged features and their cross shore and longshore scales. This technique is also excellent for determination of sea level location. Large wave breaking tends to skew the bar crest location offshore, and residual foam tends to skew crest location onshore.

Aagaard and Jorgen (1989) used a video technique to measure run-up. This was primarily an extension of Holman and Guza's work (1984). Aagard and Jorgen made use of a video camera which was mounted on a tripod and set to look alongshore. Stakes were set at specific intervals for later profile identification. The camera range was determined to be about 75 to 100 m for 15 m swash excursions and 0.5 inch diameter stakes. Frames were digitized with a PCVision frame grabber, and the profiles were scanned by the computer at selected intervals. An operator subjectively digitized the shoreline. A 2048-point time series could be generated in about 75 minutes. The authors found this method to be more time-consuming than Holman and Guza (1984) but more accurate and easier than using photographs.

The group at Oregon State University continued work into the 1990s but began to move into other applications of video monitoring. Holman et al. (1990) improved upon the previous run-up experiments during SUPERDUCK'86. Three video cameras were mounted 43.2 m above mean sea level. Video records of 1 hour and 55 minutes were taken to coincide with in-situ current meter data runs.

An Imaging Technology 150 Series image processing system was used for analysis. The appropriate geometry of the image was solved, cross shore profiles were taken at 10 m intervals, and the location of the swash excursion located each second. This use minimized the operator subjectivity of other experiments to date. Typical

horizontal resolutions were found to be 20 cm at close range (2 cm swash elevation) and 73 cm for the most distant transects (7.3 cm swash elevation).

Holman, Lippmann, O'Neill, and Hathaway (1991) investigated a video method for measuring beach profiles. This technique relied heavily on the photogrammetric transformations for the quantification of three dimensional quantities from a two dimensional image. Where most other applications had been used to determine quantities on a plane (the sea surface), this technique required an extra piece of information. A line had to be drawn across the beach profile in order to successfully extract the three dimensional data desired. A fire hose was used for initial tests, but suggestions were made for use of a light beam or shadow which could easily be automated for computerized measurements.

Results for the typical camera setup (angle of tilt = 75°, elevation = 44.02 m relative to MSL, field of view = 30°) show a 5 cm accuracy at a range of 100 m. The advantage was noted to be the ease of measurements on a large scale.

Lippmann and Holman (1991) used video to observe phase speed and angle of breaking waves. Experiments were conducted during the DELILAH experiment in fall 1990. Up to 8 cameras were deployed, but the data presented made use of only one particular camera view. Intensity records were sampled over 2 hours at 10 Hz, and later resampled at 8 Hz for easier correlation with other in-situ instrumentation. In-situ instrumentation included an array of pressure sensors and current meters.

Results of this experiment showed a good correlation between the in-situ wave measurements (phase, celerity, and spectra) and the video intensity time series. This result allows the video technique to be used for measurement of nearshore wave parameters, without the normal problems of deployment and maintenance of standard in-situ instrumentation.

A final technique was tested in 1991. Holland, Holman, and Sallenger (1991) used video to measure barrier island overwash in Isles Dernieres, Louisiana. Data were

taken along with in-situ instruments. The new data set included a major event courtesy of Hurricane Gilbert, September 1988. Overwash velocities were mapped from the video data, by calculating bore speeds from observations of gradients in the video intensity data time series.

Many coastal measurement techniques are available with video monitoring. Some areas have been studied in detail, primarily the basics of video photogrammetry and the time exposure techniques, by Lippmann and Holman (1987 and 1989). Most of the investigations have concluded with as many questions as solid results. The results are based on relatively small data sets. Comprehensive, high quality video data sets and enthusiastic investigators are required to propose and evaluate new analysis techniques.

CHAPTER 2
DATA COLLECTION

2.1 The Video Monitoring System

2.1.1 Introduction

The video monitoring system came into existence with the desire to use visual media to make observations and measurements on the assembly line or in the field. Still terrestrial and aerial photography have both been utilized for many years. For the measurement of static subjects, these methods are fine. Problems arise, however, when a dynamic event has to be documented. Video allows data to be taken continuously or in bursts. The other factor influencing the development of the video monitoring system is the financial advantage. Aerial photography can get quite expensive, with a conservative minimum around $75 per hour of flying time plus camera equipment. If multiple photos are required on a regular basis, the cost will easily exceed the cost of the video monitoring system. A video monitoring system provides the opportunity to acquire images, still or moving, at any desired sampling frequency. Maintenance is minimal after initial deployment and mainly involves periodic data off loading.

2.1.2 Description

The video monitoring system has gone through a major metamorphosis during this project. The video monitoring systems (hereafter referred to as VMS) which have been used during this project have been designed by Erdman Video Systems of Miami Beach, Florida. Erdman's VMS consists primarily of off-the-shelf consumer and industrial components which are controlled with commercial and custom software. VMS primary components include a Hi8 video camera with variable zoom, a pan and tilt mechanism which consists of a digitally-controlled stepper motor, and a personal

computer (PC). Our first VMS was run by a Databank 386 PC with only 40 megabytes (MB) of hard disk space. The current configuration uses a 200 MB hard drive, which can store up to 7000 compressed images.

VMS software allows the user full control of the camera. Up to 34 different scenes can be programmed at a time. The user sets the desired pan, tilt, and zoom for each scene. Repeatability is better than 0.1° for all angles. Sampling frequency is also set for each scene. All of the programming functions can be adjusted from a remote PC connected to the VMS by a modem. Images are acquired and digitized in 24-bit color Targa format. Acquired image data can also be transmitted to and viewed on a remote PC via the modem connection. Images are compressed with JPEG compression to maximize storage and minimize modem transmission time. All that is required for viewing purposes is an appropriate SuperVGA display. Images are decompressed and converted to standard 8-bit GIF format for display on PCs with limited display capability.

2.1.3 Capabilities

The VMS is versatile. The camera can be mounted on any wall or roof. The housing is weatherproof for outdoor deployments and includes a cooling fan and sun shroud. The only extra protection to be provided might include a lightning protection device if the system is mounted on a rooftop or lightning prone area, like Florida. Views can be set for any zoom, pan, and sampling scheme.

The first VMS (VM-1) did not include a weatherproof camera and had to be deployed inside a building. Problems arose from the occasional dew formation on the windows and typical afternoon glares off the glass windows. VM-1 recorded all video data on Hi8 videotape. Several scenes were digitized with the frame grabber for transmittal to the university for site evaluation at regular intervals. Consequently, data sequences used for analysis had to be digitized from the source tapes.

The latest version of the VMS includes a surveillance-type camera housing which is fully weatherproof. In addition to recording all data on tape, the images are digitized,

compressed, and stored on the computer hard drive. The only disadvantage exists if the user desires continuous video or a very high sampling frequency. In this case, the Hi8 taping system would be modified accordingly. The latest VMS also includes an improved pan and tilt mechanism for reliable repeatability of pan and tilt values.

Field applications of the VMS are not limited to subjects in the coastal environment. The nature of the VMS lends itself to long term monitoring projects, at a minimal cost. Other applications include construction site monitoring, breakwater stability monitoring, marine and terrestrial traffic monitoring, surface pollution dispersal, sea turtle nesting, and bird nesting behavior. The Department of Coastal and Oceanographic Engineering is currently investigating the uses of video monitoring underwater, for observing field instrumentation sites during deployments.

2.2 Field Deployments

2.2.1 Hollywood Beach

The video monitoring data from Hollywood Beach, Florida was collected as part of a study on the influences of beach nourishment on nearshore turbidity. The study, sponsored in part by Florida Sea Grant, took place between January 1990 and April 1992 in order to make measurements before, during, and after a beach nourishment during the summer of 1991. In-situ measurements of wave climate and turbidity in the lower 1 meter of the water column were recorded during 30 minute bursts at 4 hour intervals. The VMS was initially installed as a test for future projects. At the onset of the project, there was no specific goal in mind for the video data, other than perhaps site documentation. Here it is stressed that since no specific goal existed, the required attention to the details of installation, camera geometry, and ground surveys was not given. As the investigators made routine remote logons and observed the VMS data, it was realized that this was an excellent source of information pertaining to events in the coastal environment.

The Hollywood VMS was set up on the 21st floor of the Summit Condominium, located at 1201 S. Ocean Drive, Hollywood Beach, Florida. As stated previously, the camera was not weatherproof and was erected inside a private residence in the condominium south tower, 55 m above mean sea level (MSL). The camera view was pointed in a northeastward direction, over a 6.5 mile stretch of coastline including part of the project area and Dania Beach. The wide camera view (8.5 mm zoom) provided for a "useful" video window that spanned DNR R-Monuments 114 through 117 on Hollywood Beach. A maximum angle directed offshore (relative to longshore, generally N 5° E on Hollywood Beach) was about 75°, limited by the north-facing sliding glass door. Data was sampled at the following rates. Eight scenes were set at various intervals up the beach (northeast) with appropriate zooms. Video records of 0.7 seconds each were sampled at 30 minute or 1 hour intervals from April 1991 through November 1991. Figures 2.1 and 2.2 show a typical view from the Hollywood data set and an aerial snapshot with the VMS location indicated on it, respectively.

Figure 2.1 Typical image from Hollywood Beach data set

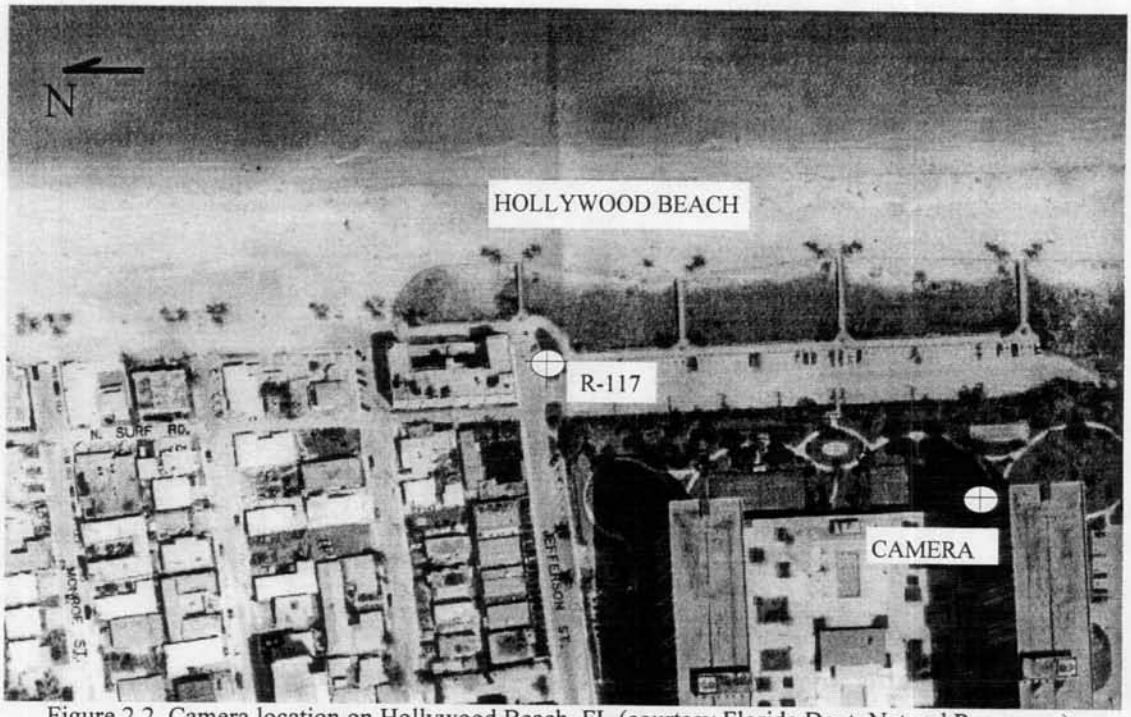

Figure 2.2 Camera location on Hollywood Beach, FL (courtesy Florida Dept. Natural Resources)

2.2.2 Miami Beach

The purpose of the Miami Beach VMS deployment was to obtain a video data set of nearshore features and their changes over several months. This deployment included several upgrades (hardware and software) to the VMS. Hardware upgrades included a weatherproofed camera housing, a much improved pan-and-tilt mechanism, and a larger, 200 MByte hard drive on which to store images. Software upgrades were fourfold. The remote access program was modified to allow the remote user to actually set and reset any scene, or add scenes as desired. The image transfer options were expanded to include transmittal of sequences of images or mosaics of images. The 8mm tape was abandoned. Images were digitized in real time and compressed and saved on the computer hard drive. This eliminated the extra step of re-digitizing desired images from tape at a later date. Perhaps the most important modification was the implementation of a time averaging scheme in order to eliminate high frequency signals and enhance quasi-static nearshore

features, like shoreline position and bars. This concept of time averaging is discussed in more detail in Section 3.1, Digital Image Concepts.

The VMS was erected outside an apartment on the 16th floor of the south wing of the Roney Plaza, located at 2301 Collins Avenue, Miami Beach, Florida. The camera height was about 50 meters above MSL. The other camera view parameters were similar to that of the Hollywood Beach deployment. Cameras are generally set for the best view during any deployment, so parameters may vary accordingly. Instantaneous images were digitized once per hour for each of 5 scenes. Time averaged images of each scene were also sampled at hourly intervals. The time averages were sampled as follows, dictated by the computer hardware and software speeds: 8 images were sampled over a 5 minute period and digitally added to obtain the final image. The image data were collected over a six month period, from December 1992 through May 1993. It is noted here that no in-situ instrumentation was deployed during the video deployment. A nearby University of Florida Coastal Data Network (CDN) instrument package was not in operation during the experiment. The primary objective was to test the application of the VMS, not to study any particularly detailed mechanics of nearshore processes. Figures 2.3 and 2.4 present a typical view from the Miami Beach data set, and an aerial snapshot with the camera location indicated on it.

2.2.3 Longboat Key

In June 1993, a video monitoring system was erected on a condominium on Longboat Key, Florida, as part of a beach nourishment monitoring program. The video monitoring program was mandated by Florida Department of Environmental Regulation. The study is designed to provide a comprehensive turbidity analysis before, during, and after the beach nourishment which occurred during summer of 1993. This paper does not cover any of the experimental details or future analysis of the Longboat Key results, but the techniques discussed herein are being applied to that data set.

Figure 2.3 Typical image from Miami Beach data set

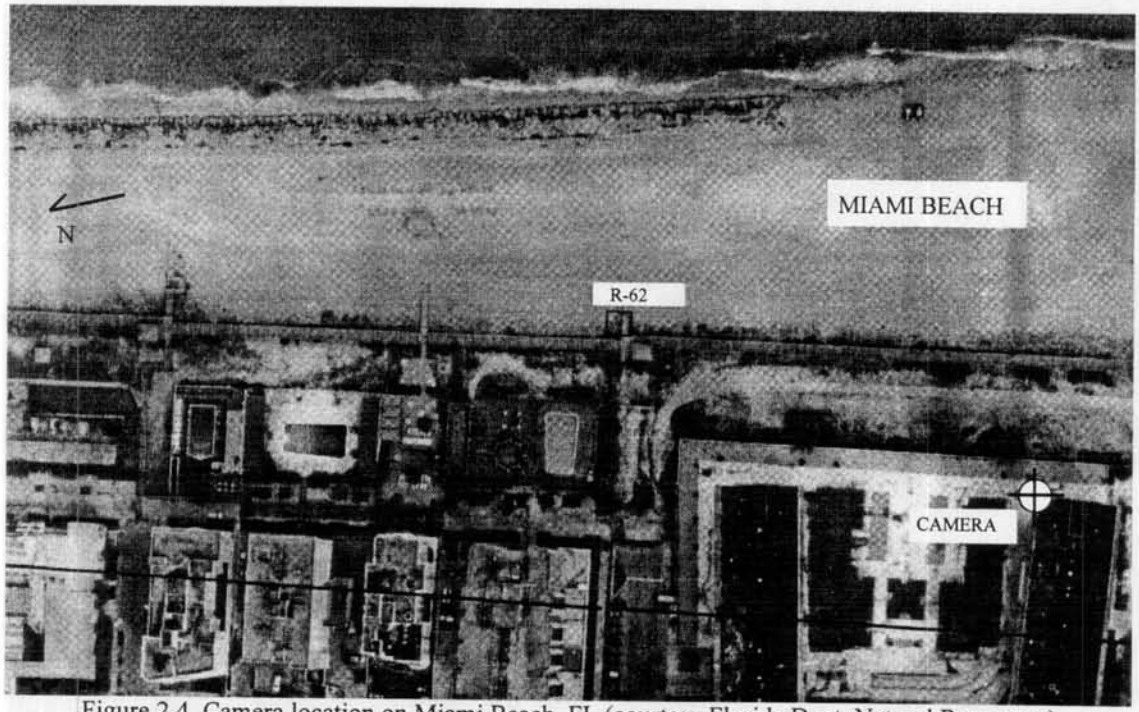

Figure 2.4 Camera location on Miami Beach, FL (courtesy Florida Dept. Natural Resources)

CHAPTER 3
IMAGE ANALYSIS

3.1 Digital Image Concepts

There is a great deal of literature on digital images and image processing. One general image processing reference is Gonzalez and Wintz (1987). In this section, a brief introduction to key concepts and terminology needed for understanding this paper is presented. Readers are strongly recommended to check the reference listing for further information which goes beyond the scope of this paper.

Digital imagery results from the desire to enhance existing pictorial information and allow computers to interpret pictorial information. A digital image is created by segmenting a picture into discrete spatial elements, hereafter referred to as pixels. Each pixel is assigned an intensity level or color. A monochrome or grayscale image consists of a matrix of pixels that have brightness or intensity values ranging from black to white. We call this a purely black and white image if only 2 grayscale shades are present: black and white. Typical monochrome images contain 256 grayscales, where 0 corresponds to black and 256 corresponds to white. Using computer terminology, an image with 256 grayscale is referred to as an 8-bit image (2^8 shades of gray), which is an industry standard. Color 8-bit images allow use of 256 colors out of a possible 16 million. Most image processing involves only monochrome images, since color adds an extra complication.

The typical image file types which were used in this study are of three types, TIFF, GIF, and BIF. TIFF (Tagged Interchange Format File) and GIF files are industry standards for personal computers, paint packages, scanners, and image processing packages. Each file contains coded pixel intensity or color data and a header with

information about the image size and other characteristics. Most images used correspond to standard VGA or NTSC monitor resolution with a size of 640x480 pixels. A 640x480 TIFF or GIF 8-bit monochrome image occupies 307 KBytes of memory. Some applications produce 512x480 images, which occupy 245 KBytes. Image storage and handling can present problems for computers with limited memory and speed.

To access pixel intensity data, these standard file formats must be converted to raw data files. BIF (Binary Information File) files contain only raw data. This binary data can then be converted to ASCII format and accessed directly by the particular user. All image conversions of this type can be done with software programs like *Image Alchemy*, by Handmade Software, Inc.

To convert videotape or live video camera signals to digital images, a frame grabber is used. A frame grabber digitizes an incoming video signal by converting the analog input to a digital output. Many frame grabbers have onboard memory buffers which can convert and store images in real time, or 30 Hz for standard video. This study utilized a Data Translation DT-3851 Frame Grabber in a Gateway 2000 486DX/50E for digitization from the Hollywood Beach data videotapes (480x640 images) and a Digital Vision Computer Eyes Color Frame Grabber for real time digitization in Miami Beach. Miami Beach images were later converted to monochrome for analysis.

Image processing involves basic operations on images, like contrast and brightness adjustments, as well as more complicated operations like filtering and edge detection. Our image processing system centers around a Data Translation software package, Global Lab Image. This software operates under a windows environment and provides simple display and advanced processing functions. It is also programmable for user customization.

Some important image processing functions include equalization and contrast stretching, intensity profiling, distance determination, image arithmetic, filtering, and edge detection. Equalization and contrast stretching are important for human perception

of image data, by allowing the user to adjust contrast and brightness for optimal visualization of image features. The computer can equalize the image using linear histogram equalization. Intensity profiling provides a plot of image intensities along a line of pixels in an image. Distance determination is used to calculate pixel-to-pixel distances for calibration with real world values. Image arithmetic includes addition (averaging), subtraction, multiplication, division, and logical operations on images. Filtering essentially applies a mathematical filter (like low pass or Sobel) to image data, which can help extract information that is otherwise difficult to see. Edge detection is a filtering process which locates edges of objects that have similar intensity or size characteristics, or user defined threshold values, which are characteristic of edges in images.

Several of the above mentioned image processing techniques will be explained in greater detail in upcoming sections. Many of the particular applications of image processing require custom implementation. Most programmers favor the C programming language, since it is well suited for high speed numerical calculations. The computational software package MATLAB, by The Math Works, Inc., is somewhat slower than C but has advantages including an ability to store and perform operations on large data sets (like images), as well as numerous routines for signal processing and image manipulation and display.

3.2 Photogrammetry Basics

The image interpretation process is based on the geometry of photogrammetric principles. The location of any point on the image is related to the location of its corresponding point on the ground, the focal length, the camera tilt, swing, and azimuth, and the exposure station elevation. This can be expressed as

$$(x,y) = f(X,Y,Z, f_c, \tau, \phi, s, H) \qquad (3.1)$$

where x and y are the image coordinates (relative to the fiducial coordinate system), X, Y, and Z are the corresponding ground coordinates to be imaged, f_c is the camera focal

length, τ is the camera tilt (upward from vertical), ϕ is the camera azimuth, s is the swing angle (or roll angle) of the camera, and H is the elevation of the exposure station above the ground plane origin O, called the nadir point. Focal length f_c is defined as the perpendicular distance (in mm) from the optical center of the camera lens to the imaging surface of the camera. For a standard camera, the imaging surface is film. For a video camera, the imaging surface is a charge-coupled device (CCD). A short focal length, say 8 mm, results in a wide field of view, while a longer focal length like 80 mm results in a "zoomed" view. Figure 3.1 illustrates the geometry of the exposure station.

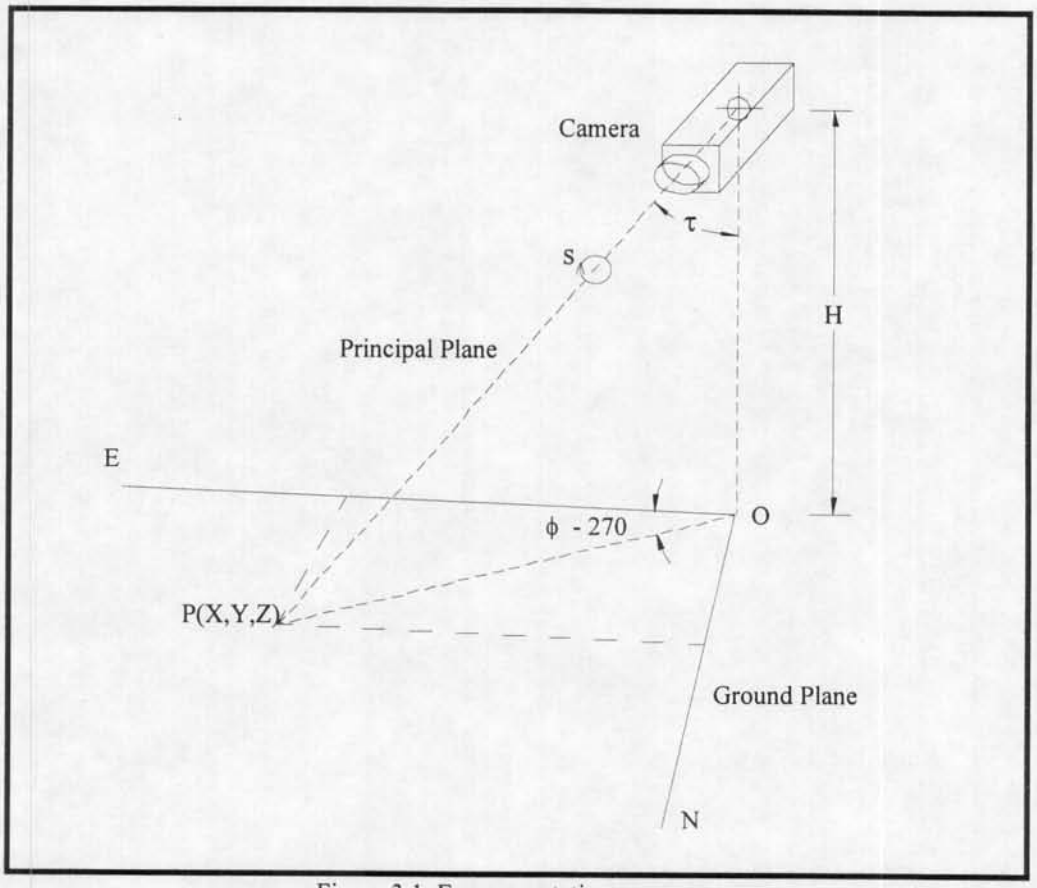

Figure 3.1 Exposure station geometry

For the simplest case, we intend on imaging (and rectifying) the nearshore sea surface. In this case the ocean surface is assumed to be a plane. The three-

dimensionality of the onshore features in the oblique image can be used for determination of the parameters of exterior orientation, but will not be accurately mapped to the rectified image (remember that this transformation applies only to a plane). Radial lens distortion should not play a major role in the rectification, so long as one does not travel too far into the distance and the edges of the oblique are avoided. An exposure height of 55 m ~ 180 ft is too low to result in any significant radial lens distortion, according to Wolf Figure 5-17, p.102 (1983). Lippmann and Holman (1989) presented the equations for geometrical transformation from image to ground coordinates. For the simple case, image coordinates p(x,y) corresponding to any ground coordinate P(X,Y,Z) can be expressed by:

$$y = f_c \tan\left(\tan^{-1}\left(\frac{Y}{Z}\right) - \tau \right) \qquad (3.2)$$

$$x = \left(\frac{y^2 + f_c^2}{Z^2 + Y^2}\right)^{1/2} X \qquad (3.3)$$

where Z denotes the relative height of the particular point P with respect to the camera elevation H, or $Z = H - Z_p$. Z_p is defined as the elevation of point P with respect to the ground plane. The application of one known pair of points (x,y) and (X,Y,Z) can be used to solve for the unknowns f_c and τ. The camera parameters f_c and τ are difficult to measure accurately. The focal length of the camera is unknown because one does not measure quantities directly from the CCD, but from a computer screen which has an enlarged display. Thus the camera focal length is altered by an unknown value. By applying several of the surveyed control points to eqns. (3.2) and (3.3), the unknowns can be determined with the method of least squares which results in the "best" solution.

More complicated solutions result when the scene geometry deviates from the simplest case. For our case, most of the useful images from Hollywood Beach fall into

this complicated category. The horizon line is not parallel to the reference axis (say, the top edge of the image), but is tilted at some angle. Using the rigorous but generalized equations for the solution of high oblique images (Wolf, pp. 442-453), the geometry can be solved numerically. However, Wolf points out that the relationships governing the image-to-ground transformation problem can be based on three independent angles. The idealized problem equations (3.2) and (3.3) account for the tilt angle. The other angles, swing and azimuth, can be accounted for outside equations (3.2) and (3.3).

The azimuth angle ϕ is determined from survey data or estimated and solved as done previously with control points and least squares. Solution of f_c, τ, and ϕ with these methods results in typical errors up to 0.5 percent, 0.25°, and 0.5° respectively (Holman and Lippmann, 1989). The swing angle can be accounted for with a basic rotation of the oblique image to effectively "untilt" the horizon. Technically, this process is called converting the fiducial coordinates (x,y) of the image to the appropriate auxiliary axes (x',y'). Figure 3.2 defines the image coordinate system. Since (3.2) and (3.3) perform the transformation in the idealized camera coordinate system, the results of their application lie in the auxiliary image coordinate system, and must be converted back to the fiducial coordinates. The swing angle s is defined as the angle between the fiducial vertical axis and the downward end of the auxiliary axis that is perpendicular to the apparent horizon line. The swing compensation results from a simple coordinate rotation.

$$\begin{aligned} x' &= x\cos\theta - y\sin\theta \\ y' &= x\sin\theta + y\cos\theta \end{aligned} \qquad (3.4)$$

The application of (3.4) accounts for the swing angle, if present, where $\theta = s - 180°$.

3.3 Image Rectification

3.3.1 Introduction

Rectification of images is not a new concept, but it is essential to the successful analysis and interpretation of oblique images. The basics of image rectification can be

found in any text on photogrammetry. Rectification involves the transformation of an oblique image into a plan (or map) view by graphical or analytical methods.

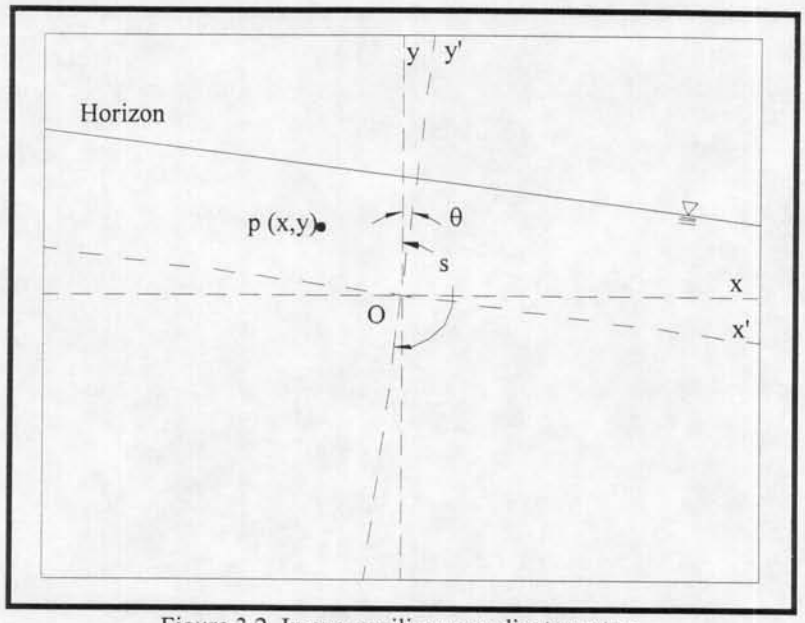

Figure 3.2 Image auxiliary coordinate system

Oblique images are difficult to take measurements from, due to the varying degrees of perspective distortion. What one believes to be, for example, a line running east to west may be at some unknown angle. For this reason, a rectified image can provide much needed spatial information which cannot be accurately determined from an oblique image. The current goal is to produce a rectified image of the sea surface which is on a scaled, square grid. Spatial variations of nearshore features can then be easily observed and measured for research in the coastal environment.

The rectification process is fairly straightforward once the geometry of Section 3.1.2 is understood. The parameters of exterior orientation are solved, based on the control points and method of least squares. The next step is to determine the desired output resolution and location of the rectified view on the original image. This step is

best left to trial and error. After the output image "grid" and scaling are set, the rectification can begin. Each rectified grid point P(X,Y) is transformed through (3.2) and (3.3) to determine the corresponding image location p(x,y). The intensity found at location (x,y) is mapped to (X,Y). This process is repeated for each grid point, or each pixel. The loss of resolution is readily apparent with an understanding of the rectification procedure. Many points in the far field of the rectified grid will receive intensities mapped from a single point on the oblique image. Results are satisfactory but may be improved with enhanced image processing techniques (averaging or bilinear interpolation) during the mapping process.

The final rectified image is on a scaled grid of known dimension. Direct measurements of desired length scales can be made with the use of graphical techniques or an image processing package.

3.3.2 Program background

The program *rectify.m* was written for math package MATLAB for several reasons. Primarily, MATLAB can support the large data arrays (three 640x480 image matrices) which are required to solve the problem. When using a PC-486 computer, a typical black and white image takes about 25 minutes and 9 MB of active memory to rectify. Careful attention to survey work for the ground control (or ground "truthing") of the images is imperative to obtaining the most accurate rectified images. Resolution of the rectified image depends on the height of the camera above the plane of rectification (mean sea level for my application), the tilt angle of the camera, and the focal length (zoom) of the camera lens. The following paragraphs describe each step of the procedure and program.

3.3.3 Camera and view setup

The camera setup and views are left to each user, but several factors must be kept in mind. First, the camera should be weatherized and placed outside so reflective effects of windows and dew do not ruin potentially important data (the author recommends

Erdman Video Systems, Miami Beach, FL for the solution of all video installation and sampling requirements). Second, the camera view should be set so the apparent horizon line is tangent to some horizontal reference to avoid roll effects in the rectified images. This roll effect complicates rectification and had to be addressed in the Hollywood Beach data set. Third, the study area should be split into several longshore/cross-shore segments and the zoom power of the camera utilized. A zoomed image in the distance will produce better results, although the ground survey work will increase with each new scene. Care should be taken when using zoom features of cameras that are not purchased with video monitoring packages. Each scene's zoom factor must be consistently duplicated to avoid re-calibration of focal length and tilt for all images.

3.3.4 Surveys and measurements

After setting up the camera and determining the sampling scheme, measurements of the so-called parameters of exterior orientation should be performed as carefully as possible. The desired parameters include: camera elevation above a standard reference elevation (1929 NGVD for our purposes), camera focal length for each scene, and the tilt angle of the camera axis upward from vertical. Next, ground control points must be determined (as applicable to the particular setup geometry) and surveyed. For completeness, one should survey a minimum of 4 points with as much spatial coverage of the camera view as possible. It is best to utilize permanent features which are easily seen in the view and tied into standard survey monuments (like DNR R-monuments). The azimuth angle ϕ between the camera system x-axis X_g (perpendicular to the camera view) and the ground system x-axis E (usually directed offshore) needs to be determined. Estimate angle ϕ and survey several points relative to both coordinate systems (these can correspond to the above ground control points). Finally, survey the point which corresponds to the center of the camera view, if possible. As a general rule, the more points surveyed will produce the best final results. The author again emphasizes the importance of thorough surveys.

Another useful tool for the verification of the rectified images is the aerial photograph. If recent aerials are not available, it is recommended that several aerials of the study area be taken. The study site and camera location should be clearly indicated or obvious to the naked eye on the photographs. Flags, bright buoys, and boats are good site markers. These photographs serve as a basis upon which the rectified images can be ground truthed.

3.3.5 Rectification program

The rectification program is versatile; it can be used for any image size, typically 640x480 or 512x480 images. The program has 2 parts: *rectify.m* can be run when a new camera setup or view is implemented. The parameters of exterior orientation and output grids are determined and saved as two MATLAB files *inp.mat*, containing the camera focal length f_c, tilt angle τ, elevation H, image size and resolution, camera azimuth angle ϕ and the offsets of the output grid in camera coordinates, x_o and y_o. The offsets x_o and y_o are distances from the camera coordinate origin to the standard ground coordinate system origin, measured in the camera coordinate system. File *inp2.mat* contains the ground location grids (Xg and Yg) of the rectified image in camera coordinates. The second part, *remap.m*, can be used after the initial run of *rectify.m*. *Remap.m* loads the two input files so the input phase of the original program is bypassed.

When running *rectify.m*, the user is prompted for various inputs, including initial guesses for f_c, τ, ϕ, θ (if required), and control points. All input data must be entered in array column form in consistent units. The first part of the program solves for the parameters of exterior orientation by applying the method of least squares to the known survey control points. More points spread over the expanse of the screen increases the accuracy of the results. The second part of the program sets up the rectified image grid and loads the input image. The final part of the program applies the image transformation equations and maps the correct pixel intensities to the final image grid.

The calculated focal length will depend on the image size being used. If one was to measure distances directly from a 1:1 positive, the focal length calculated by the program would be the focal length set on the camera's zoom lens. However, we will generally measure image coordinates in pixels from a digitized image on the computer screen, so the calculated focal length will be considerably larger than the camera's actual focal length. The particular computer screen will have to be calibrated. In doing so, one essentially determines the size of each pixel. Image coordinates measured in pixels can then be converted to proper units within the program.

The output resolution and location of the final grid origin are user inputs. The output image resolution (meters/pixel) can be any value depending on the detail required. I have used resolutions of 1 m/pixel and 2 m/pixel for most cases. Figures 3.3 and 3.4 present an example of a digitized oblique image from the Hollywood data set and the corresponding rectified image at 2 m/pixel resolution, respectively. The output grid origin is moveable so that one can effectively "window" an entire image to create a mosaic of more detailed images. Remember that the output resolution degrades fairly quickly with increasing distance from the camera nadir point and increasing camera tilt.

Figure 3.3 Oblique image, Hollywood Beach 5-24-91

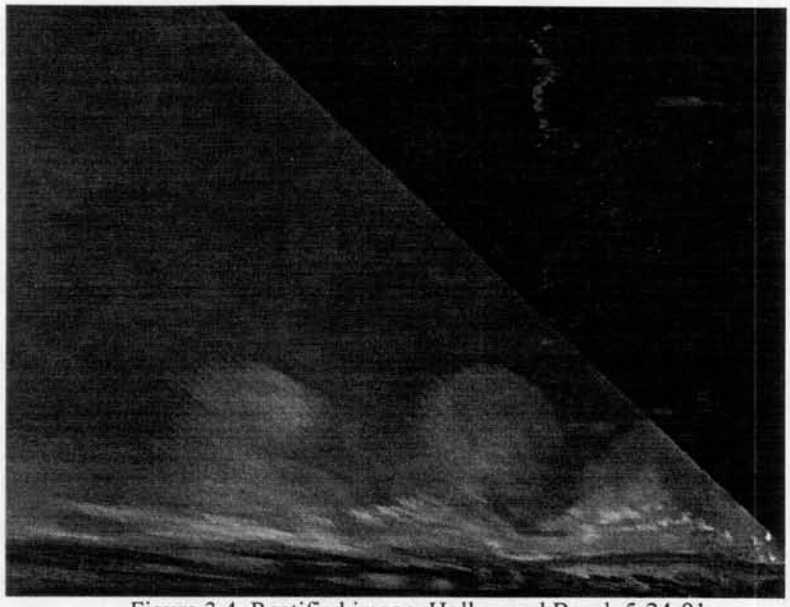

Figure 3.4 Rectified image, Hollywood Beach 5-24-91

3.3.6 Program Calibration

The rectification program was tested and calibrated before applying it to any field data. A test case was set up inside a lab at the University of Florida. A rectangle was marked on the floor, and a Hi8 video camera was set with zoom, tilt, and azimuth similar to normal field conditions. Figure 3.5 shows the test case geometry. The camera was 0.692 m above the ground plane (the floor), the zoom was set to 11 mm, and the azimuth ϕ was -27.5°. An image was digitized as shown in Figure 3.6. A straight edge was placed along the principal line of the camera view for clarification. With known control points on the ground and image, the image was rectified using *Rectify.m*. The output resolution was set to 2.5 mm/pixel on a square pixel grid. The rectified image is shown in Figure 3.7. The rectified image was loaded into Global Lab Image, a windows-based image processing software package, and checked for errors.

It was found that the RMS normalized difference between rectified image estimates and actual measurements was 5.2%. The distortion of the image in the far field is evident by observing the crispness of the bottom edges of the rectangle and the relative

fuzziness of the top edge. This distortion is due to the break down of resolution in the image as we approach the "horizon" and possibly some lens curvature effects. It is noted that although the crispness of the lines degrades, the overall thickness of the lines remains constant. The actual thickness of the tape was 1.9 cm, and the average measured thickness of the tape on the rectified image was 2.0 cm. Similarly, the actual and measured lengths of the dark-colored ruler were 0.61 m. Therefore, precise edges of subjects in the far field of the rectified images may not be accurately detected, but their location in the ground plane and relative size should be accurate. Also, the original is accurately represented after rectification. The rectangle was not precisely squared off when it was set, so the angles between the sides are not exactly 90°. Note also that the black wedges on each side of the rectified image result from the edges of the original image and define the camera field of view.

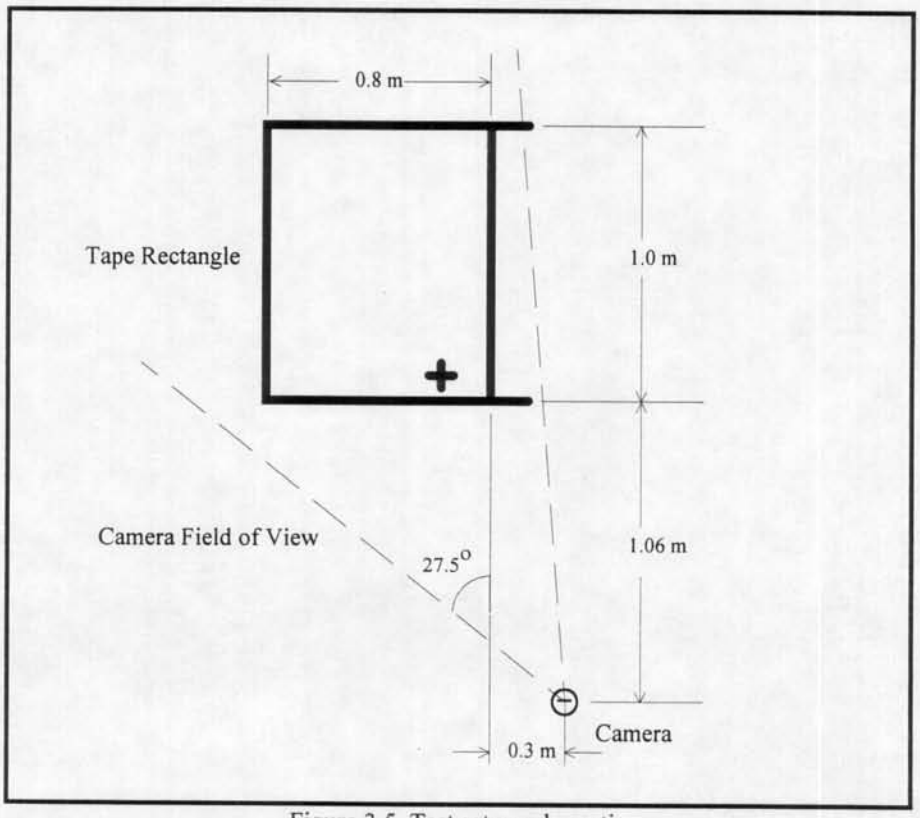

Figure 3.5 Test setup schematic

Figure 3.6 Oblique test image

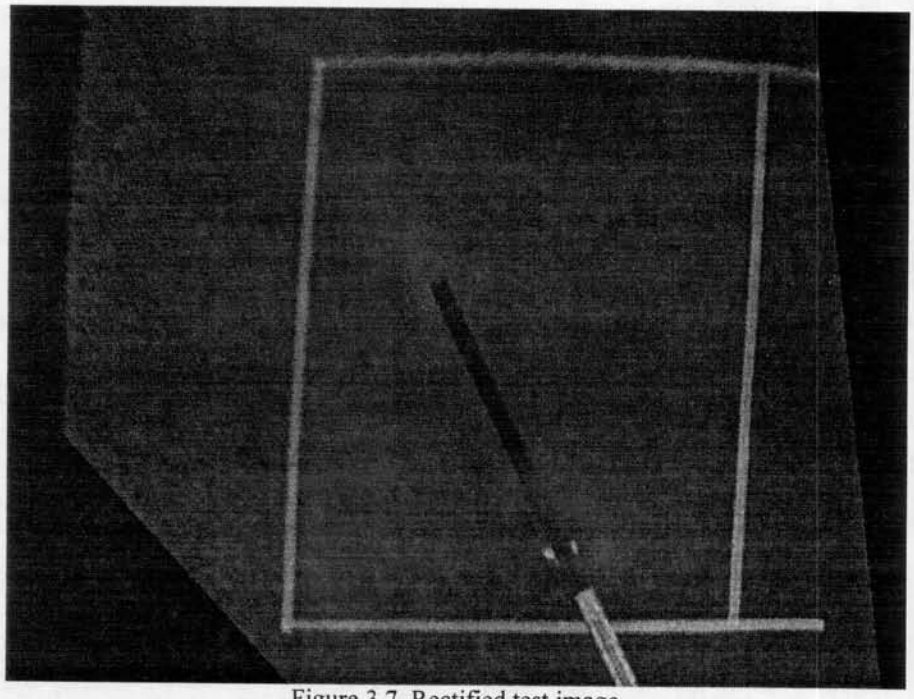

Figure 3.7 Rectified test image

A second test case was set up at Florida Field. To simulate typical field conditions, the camera was placed 9 m above the level of the field and an oblique view was taken. An Omni Total Station was used to survey locations of the known control points to determine the parameters of exterior orientation. The oblique image is shown in Figure 3.8. The image was rectified as shown in Figure 3.9. Two difficulties arose during the test which affect the result. First, the field has an 8 inch crown which is the difference in elevation between the sidelines and the centerline of the field. The camera location and large tilt angle (84°) cause a distortion of the lines as we move towards the upper right of the image in Figure 3.8. The crown causes the lines to appear more curved than a normal perspective on a plane. Second, the camera mount on the tripod was not level and was not determined until after the test was completed. The swing angle compensation (Equation 3.4) was based on the assumption that the angle of the wall on the far end of the field was parallel to the horizon line, since no other reference was available.

The rectified output reflects the true locations of points on the field with the loss of resolution typical of the rectification process and the influence of the crown of the field. Measurements were made on the rectified image to check the accuracy of the rectification program. Errors were assessed by evaluation of the RMS normalized difference between actual measurements and video-based estimates:

$$\text{RMS error} = \sqrt{\frac{\sum_{n} x_i^2}{n}} \qquad (3.5)$$

where x_i are the normalized errors between image estimates and actual quantities and n is the number of observations. For the Florida Field test case, errors were calculated with equation (3.5) as 0.77% for undistorted angular measurements and 4.17% for length measurements.

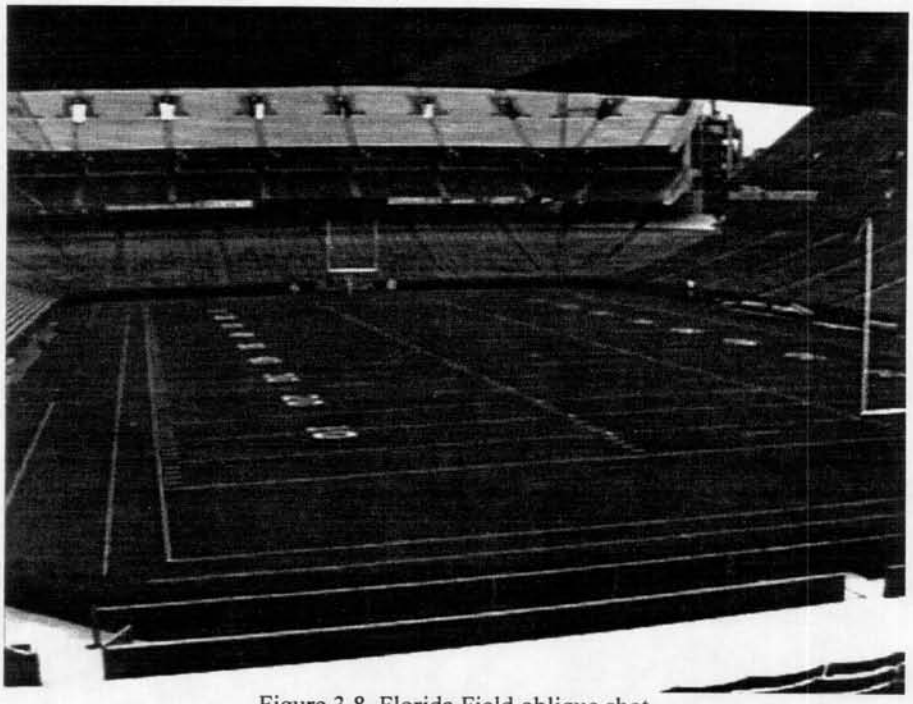

Figure 3.8 Florida Field oblique shot

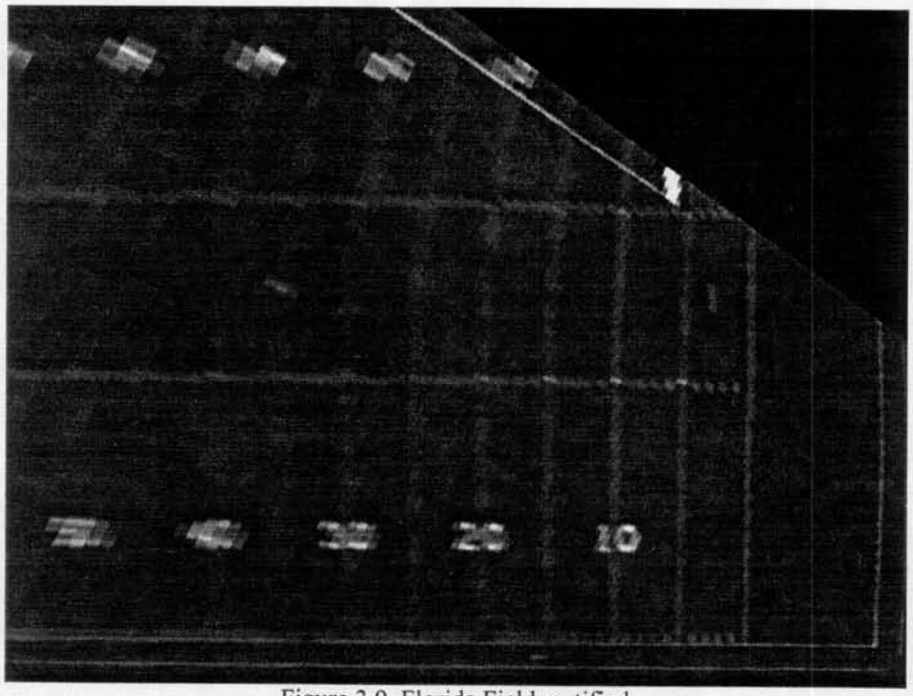

Figure 3.9 Florida Field rectified

3.4 Other Methods

Alternatives to the image rectification method are available for quantification of features in images. The two suggested methods include a calibration and measurement method with a commercial image processing software package, *Global Lab Image*, and generation of a perspective grid which is superimposed over image data. These methods are mentioned for completeness but are not actually applied. Further investigation is required to use these methods in the future.

3.4.1 Global Lab Image

One alternative method to rectification is the straight implementation of an image processing package that allows calibration. Data Translation's software package *Global Lab Image* includes functions for perspective calibration of images. The operator can pick up to eight known control points on an image and input real world two-dimensional values for them. A least squares method solves image perspective transformations, based on the input values, to produce correct distance measurements. The limitation is that the function only solves the perspective transformation in a plane. Thus, all control points and measured points must be coplanar.

This technique was attempted during the early phases of this research, but the limitations proved to be too restrictive. Measurement problems result from the large perspective distortion of the high oblique images. Even if the calibration is successfully implemented, making distance measurements from the obliques is very difficult. In the coastal views which are used here, one cannot ascertain the cross shore and longshore directions at each point desired. Drawing cross shore transects at several points along an oblique coastline view is nearly impossible. The oblique image calibration method was abandoned for this study, but may prove more useful when the perspective problem is more subtle.

3.4.2 Overlay Grids

A second measurement technique that was considered during the early phases of research was overlay grids. These grids can be constructed from analytic formulae or graphical packages which generate them. Perspective grids, unlike square grids, account for the distortion that accompanies an oblique image. By selecting an appropriate

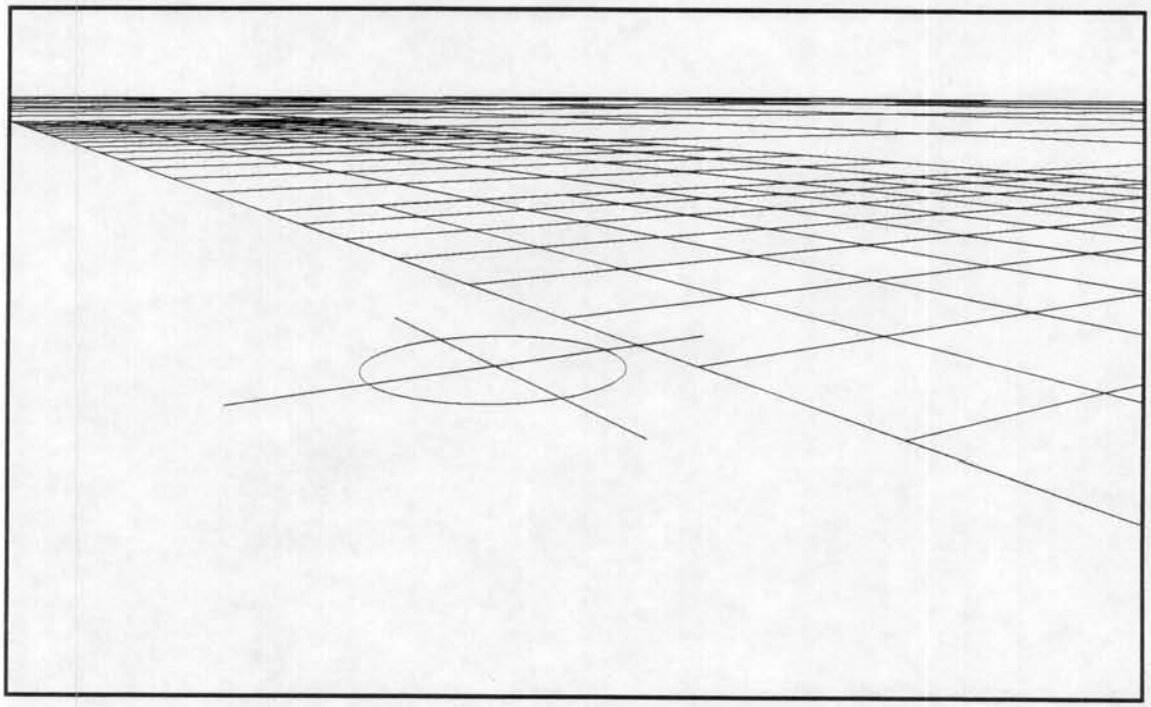

Figure 3.10 Overlay grid

reference axis (like the shoreline), perpendiculars can be constructed based on photogrammetric principles (Wolf, 1983). Figure 3.10 is an example of a perspective grid, generated by *Autocad.* To generate a grid of this type, the camera elevation and location from the reference axis must be known. Problems result during overlay procedures, as limited software is available for image overlay. This technique was also abandoned for the more versatile rectification approach of Section 3.3.

CHAPTER 4
RESULTS AND DISCUSSION

4.1 Introduction

The video data were collected at the sites and times as described in Chapter 2. Pertinent images and events were then selected for analysis, based on observation of the recorded data. Images were analyzed with the rectification method outlined in Chapter 3.

As a result of the large amount of quality data collected and varied interests of the sponsoring parties, the analysis was broken down into three major sections. First, site documentation deals with the generally qualitative uses of video monitoring and the handling of such large data sets. Second, nearshore features presents some measurement capabilities of coastal morphology which are of interest to coastal engineers, including shoreline position and sandbar identification. Third, turbidity phenomena investigates the use of video monitoring for mapping of natural and man-induced turbidity events.

4.2 Site Documentation

The first and most obvious use of video monitoring is site documentation. The simple gathering and archiving of images provides a database of valuable information. The problems which must be addressed include image storage and archiving, data extraction, and then presentation methods.

4.2.1 Image data sets

Video monitoring generally results in large data sets, since sampling can be set to virtually any frequency desired. Especially in the applications of coastal engineering, many of the processes which are desirable to record occur during relatively long time

periods. For example, sandbar morphology and shoreline change are monitored over weeks or months. Investigators want a thorough data set, so records may be taken each hour for several weeks or months. In shorter-term investigations, like rip currents or swash observations, the overall time period may be only several hours. The image sampling frequency may be once per minute, or even once per second. To be more specific, the Hollywood Beach image data set is used as an example.

The Hollywood data set consists of 11 scenes of 0.7 second video records which were recorded at 15 minute intervals. Data were collected over a 7 month period from April through November 1991. Each day recording began at 7 AM and continued until 7 PM. If we take each 0.7 second record as being one "image," (since one would probably digitize one representative frame from each 0.7 second record) then the total number of acquired images is 110,880. Due to this copious data set, only one scene was used for further analysis. The video records fill over 10 two-hour Hi8 videotapes. Original records were recorded in series on tape and encoded with date and time information. The master tapes were later "decoded," a process that involves placement of the records from each scene in chronological order. This computer-assisted process creates a time lapse video of each scene. Time lapse records allow quick viewing of scene conditions and changes over a relatively long period of time. Further image manipulation from the tape records is discussed in forthcoming sections.

The Miami Beach data set consists of eight scenes of purely digital images which are compressed with JPEG compression to a size of 30 KBytes. No tape was used, so storage and handling problems result from digital data files. In order to use images, each file must be decompressed (expanded). Image viewing software like *Image Alchemy* or *Vuimage Plus* is then used to look at the data. Several software packages allow the creation of slide shows from image sets. The advantage of purely digital images is the ease of access to any particular date and time. The disadvantages include disk storage space and the inability to see real-time activity.

Figure 4.1 Hollywood Beach under typical conditions

4.2.2 Event documentation

Without entering the quantitative realm of video monitoring, the qualitative aspects of the video data are numerous. Site documentation includes assessment of:

1. Local conditions
2. Beach traffic
3. Beach activities
4. Shoreline change
5. Predominant coastal features
6. Strange events.

Each of these items can be qualitatively estimated from the video data. Presented next are some examples of each.

4.2.2.1 Local conditions

Figures 4.1 and 4.2 present a comparison of images from Hollywood Beach to illustrate the assessment of local conditions from video data. Image 4.1 shows an up

coast zoom from late May 1991, under typical weather and crowd conditions. Typical conditions for South Florida in late May include sunny skies and calm seas. Image 4.2 is a similar view of Hollywood Beach during a large storm system that occurred between

Figure 4.2 Hollywood Beach under storm conditions

May 19 and 22. Note the wide surf zone and numerous offshore whitecaps. Winds from the southeast at 20 to 28 mph and large waves of 7 to 10 feet were reported in the dredger's log during this time period, as nourishment operations had to be postponed. An in-situ record of significant wave height (Dompe and Hanes, 1992) during late May is shown in Figure 4.3. A peak significant wave height of nearly 2 meters is quite large for south Florida. This ability to qualitatively verify in-situ measurements with the video records is a useful application of video monitoring. The video data permits a visual comparison of conditions like wave size and direction with in-situ measurements. A

video monitoring system was also utilized during the Vilano Beach experiment in spring 1992 for verification of in-situ instrument data.

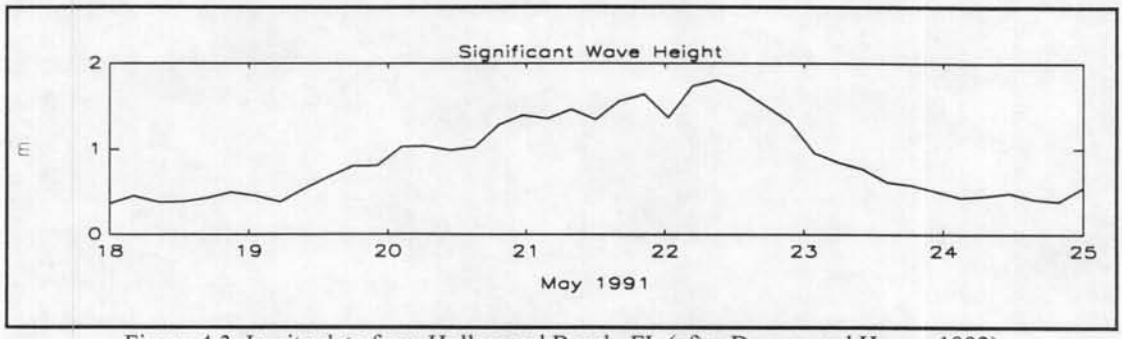

Figure 4.3 In-situ data from Hollywood Beach, FL (after Dompe and Hanes, 1992)

4.2.2.2 Beach traffic

Another general use of site documentation video records is the ability to measure beach use. In Figure 4.1, a typical day at Hollywood Beach, the number of beach goers can be estimated. Using the video or digital original for optimal clarity, people on the beach and in the water can be counted. This particular scene is far in the distance. A much better result can be obtained for the traffic application if the camera is closer to the point of interest. Knowing the area of a given beach segment, the average number of people per unit area can be determined. Of interest to government agencies may be the number of beachgoers, for cost and benefit analysis. With the beach nourishment in mind, the benefits of a wider beach can be easily quantified with the use of video records of beach traffic before and after the nourishment.

4.2.2.3 Beach activities

In addition to beach use by people, the video records present a comprehensive view of various beach activities. First is the routine beach maintenance, which includes garbage removal and sand grading. Second is the ability to document the beach

renourishment procedures (in the Hollywood Beach case). Figure 4.4 is an image from June 16, 1991. The dredge discharge was placed around 800 feet south of DNR monument T-115 from 3 PM until midnight. In Figure 4.4, one can see the discharge point in the lower right. The sand/water slurry mixture is deposited so that the dike system allows the water (and fine sediments, resulting in coastal turbidity) to escape to sea, while the higher quality sediment remains on the beach. On the left are bulldozers which grade out the newly placed sand to the specified design slope. Also in the image are the discharge pipe and temporary construction office on the beach. Figure 4.4 is only a single image. The time lapse video allows the viewer to actually see the discharge point operation and movement, the bulldozers at work, and the new beach being built.

Figure 4.4 Hollywood Beach renourishment, June 16, 1991

4.2.2.4 Shoreline change

From video records we can also make simple, qualitative analysis of shoreline change. From wide views or close zooms we can see the long-term shoreline changes as well as tidal fluctuations throughout the day. Individual images are difficult to use for this purpose and the time lapse videos are much easier for qualitative analysis. A more quantitative shoreline position analysis is discussed in Section 4.3. Figure 4.5 presents an image of the beach down close. These images were not calibrated and were not used for subsequent analysis, but the potential for detailed measurements is apparent. Swash motions are easily recorded and quantified. A detailed method is presented in Holman and Guza (1984) and Aagaard and Holm (1989).

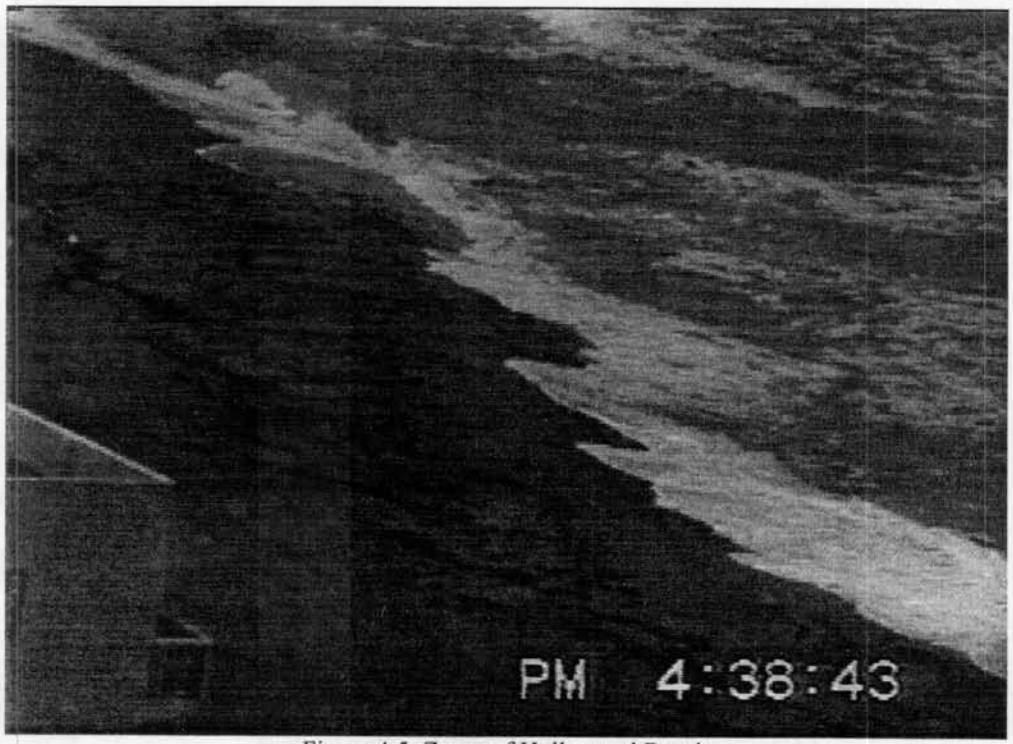

Figure 4.5 Zoom of Hollywood Beach

4.2.2.5 Predominant coastal features

Coastal features are of interest to the coastal engineer because an understanding of their formation and forcing mechanisms may reveal coastal circulation and nearshore sediment transport patterns. Field data have been collected with standard instrumentation, but the use of time-lapse video adds the advantage of being able to see changes over any period of time. Sampling frequency can be set for any observation requirements. For example, the Hollywood data set contains several views. Figures 4.6 and 4.7 present similar images taken over about a month time period. Figure 4.6 is an image from Hollywood Beach, in front of the Hollywood Beach Hotel complex, taken on April 26, 1991. Four large scale, symmetrical beach cusps can be seen along the shoreline. A large storm which occurred between May 19 and 22 effectively wiped out the cusps. Figure 4.7 shows the effect of the storm on the cusps. Figure 4.7 was taken on May 23, 1991, after the storm passed and the seas started to resume typical South Florida conditions. Other predominant features include rip currents and sandbars.

4.2.2.6 Strange events

Documentation of strange or random events is another area of qualitative video monitoring. Several examples have been discovered during this research. Most of the time, these events are not discovered until the video deployment is over and the tapes or images are reviewed. One instance occurred during a test deployment in Miami Beach. On March 24, 1991, a freighter ran aground on South Beach during a storm. The video captured the events surrounding the grounding and removal of the ship on March 31. Figures 4.8 and 4.9 show the ship when it ran aground and its removal, respectively. During the eight days that the ship remained aground, a tombolo formed between the beach and the ship. This event also created a good surf break as evidenced by the large number of surfers seen in several images (Figure 4.10). Figure 4.11 is another scene from the Miami test deployment including a bungee jumper caught in free fall. Perhaps the

Figure 4.6 Hollywood beach cusps, April 26, 1991

Figure 4.7 Hollywood beach cusps, May 23, 1991

Figure 4.8 Cargo ship grounded on Miami Beach

Figure 4.9 Cargo ship removal

Figure 4.10 Surf break after ship removal

Figure 4.11 Bungee jumper in mid-flight

most pertinent event to coastal engineering is the data from Hollywood Beach that includes the great Halloween storm of 1991. The in-situ instrumentation was not deployed during the storm, but the video monitoring system did capture the event. Figures 4.12 through 4.14 present several images from the Halloween storm. Figure 4.12 shows the large waves generated by the storm, with four discrete breaker lines. This type of wave breaking is uncharacteristic in South Florida, with the exception of winter cold fronts (which can generate large northeast swells) and tropical activity. The shorebreak and setup which caused coastal flooding are obvious in Figure 4.13. Increased fine sediment suspension results in nearshore turbidity, as shown in Figure 4.14. The greater relative intensity in the nearshore area corresponds to elevated turbidity. Also note the periodic wave trains approaching the shoreline.

Figure 4.12 Halloween storm waves, October 31, 1991

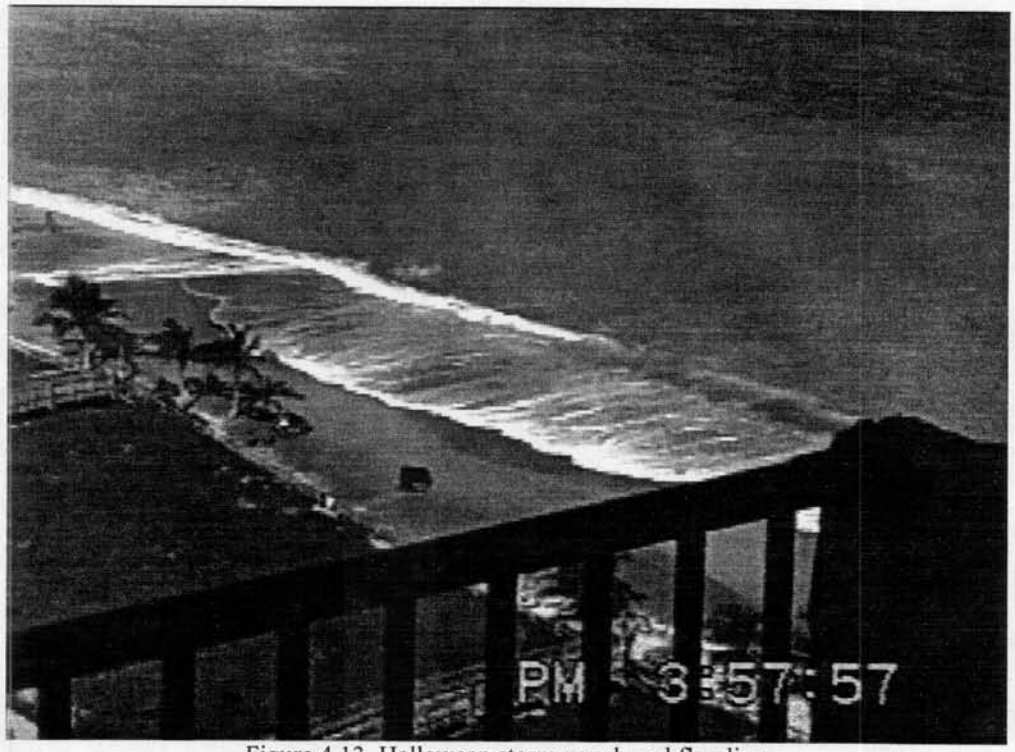

Figure 4.13 Halloween storm swash and flooding

Figure 4.14 Nearshore turbidity during Halloween storm

4.3 Nearshore Features

This section deals with the more quantitative aspects of video monitoring. The video monitoring system could be used for any specific study of nearshore features, but only the most general are presented here. The applications include mapping of the shoreline position, bars, and surf zone width. The Hollywood Beach data is used for the shoreline position analysis. The Miami Beach data, which incorporates a time averaging technique, is used for the study of bars and surf zone width.

4.3.1 Shoreline Position

Shoreline position and shape are important to coastal engineers for obvious reasons. Shoreline location is an indicator of erosion or accretion rates at a specific place. The shape of the shoreline can reveal much information about the local wave and current conditions of a particular beach. It is desired to map the shoreline remotely, over any given period. Using video monitoring, this can be done without performing time-consuming profiles or expensive aerial photographs.

The Hollywood Beach data set provided an excellent opportunity during the beach renourishment of summer 1991. Select video images were rectified at a resolution of 1 m/pixel for this section. The beach renourishment began to the south of the camera location in late April and finished well north of the site in August. Selected images include April 26, June 13 through 19 (when the dredge discharge passed by the camera site), and August 16. Figure 4.15 shows a series of images over this time, with dates indicated in the upper right of each image. The corresponding shoreline plots are graphically represented in Figures 4.16 and 4.17. Figure 4.17 shows representative shoreline positions for April, June, and August 1991. Figure 4.18 shows a representative shoreline for each day of interest when the nourishment passed the site. The cross shore distance shown is taken from a baseline along the west edge of the broadwalk on Hollywood Beach, close to the east-west coordinate of DNR Monument R-116.

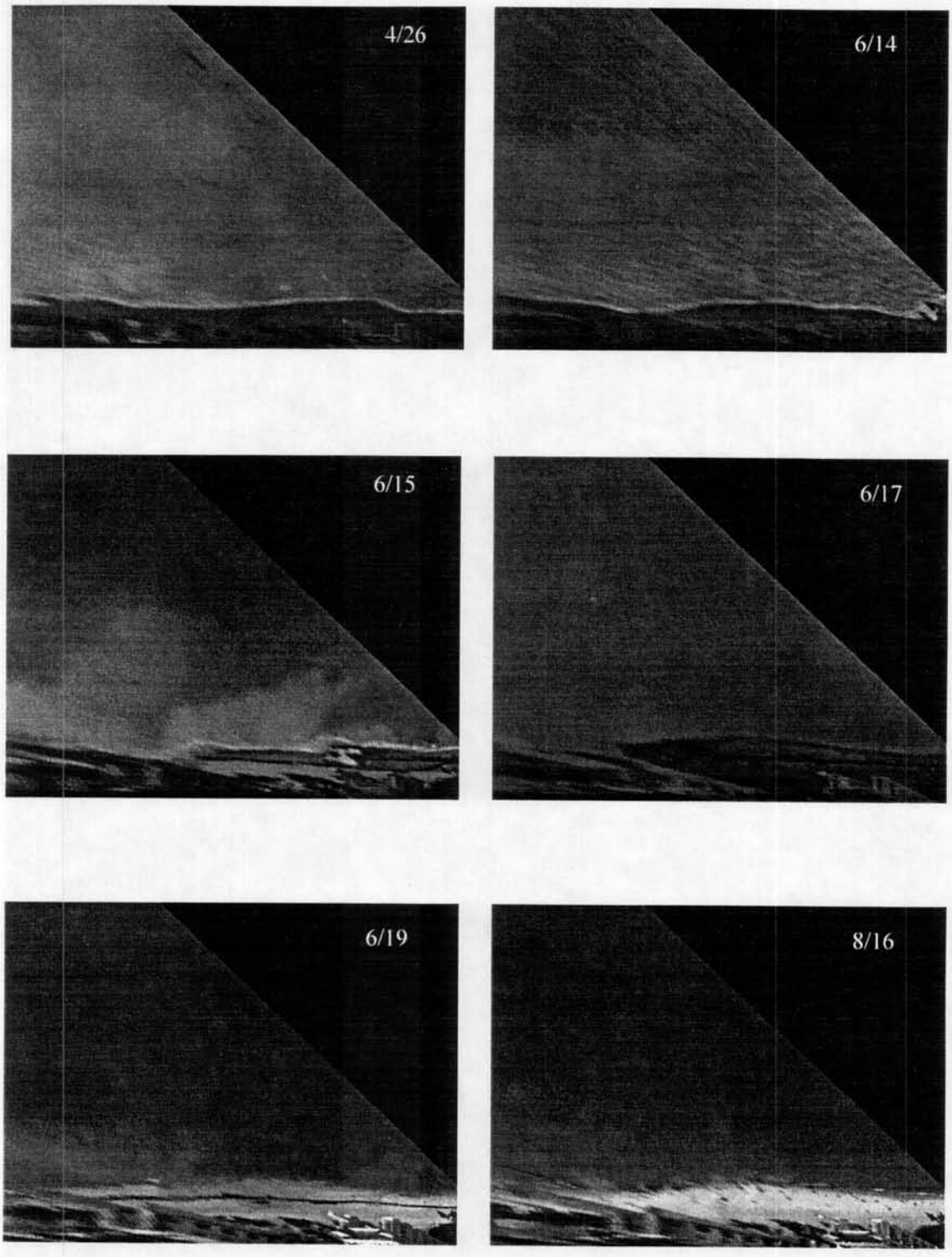

Figure 4.15 Hollywood Beach nourishment sequence

The longshore coordinate (in meters) is arbitrary, but approximate longshore locations of DNR/CP&E Monuments are shown as reference points.

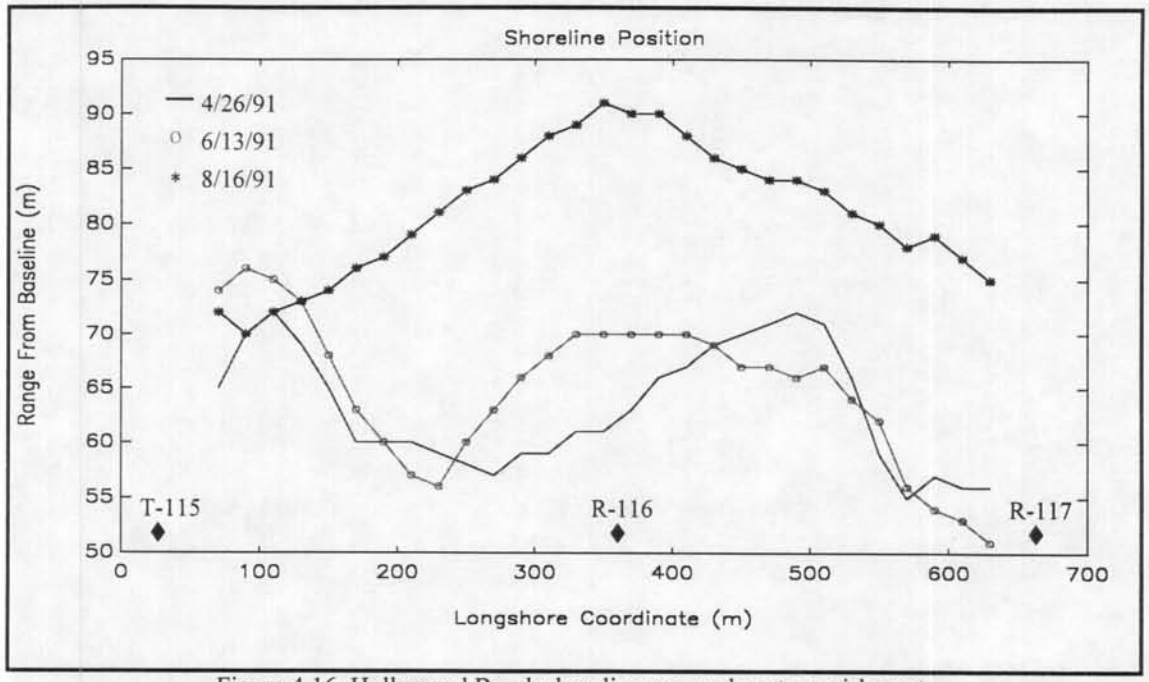

Figure 4.16 Hollywood Beach shoreline pre- and post-nourishment

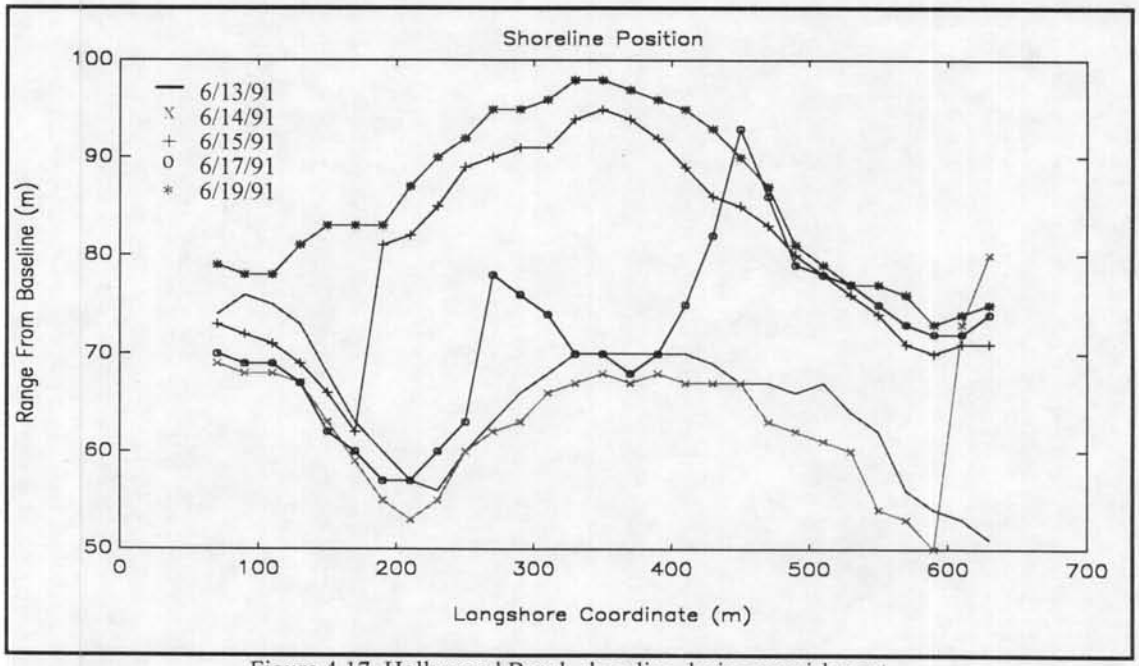

Figure 4.17 Hollywood Beach shoreline during nourishment

The reader must remember that the plots shown are digitized from a representative image on each day chosen. Therefore, the effect of swash motion and tides are not taken into account. To better represent the mean shoreline position for any particular day, an average of all the day's images should be taken. The averaged image would remove the effect of the tidal and swash motions around the mean shoreline. This method would not be suitable in this case, since the shoreline position may change drastically over only a couple of hours during the nourishment construction phase.

Qualitatively, the shoreline had a wavy or rhythmic appearance in April. The widest points occurred around T-115 and R-116.5. Significant storms occurred in May and June which reshaped the coastline as shown on June 13. The widest areas remained around T-115 and shifted from R-116.5 to R-116. After the project was completed, the area near T-115 had received the least amount of material, while the previously narrow areas received a larger fill volume. This is in general agreement with the construction plans, which show a wider toe of the fill around R-116 relative to the surrounding monuments (CP&E, 1990). According to Coastal Planning & Engineering's 6 Month Follow-Up Study (1992), moderate erosion occurred at R-116 and accretion occurred at T-115. Barring background and individual erosion events, this scenario could be inferred from the August 16 shoreline and the general spreading out of the fill.

The shoreline data can also be checked with the nourishment construction surveys that were taken as the fill was placed. Figure 4.18 presents raw fill beach profiles that were taken by the construction crew as the fill was placed. Surveys were taken on the dates shown, at the indicated monument. Specific times were not given, but the date of the profiles can be used to check the validity of the shoreline position extracted from video data. Figure 4.19 shows the shoreline position according to the construction surveys, and includes the raw fill and the graded fill. The jagged curves result from the sparse data points, which exist only at the monuments.

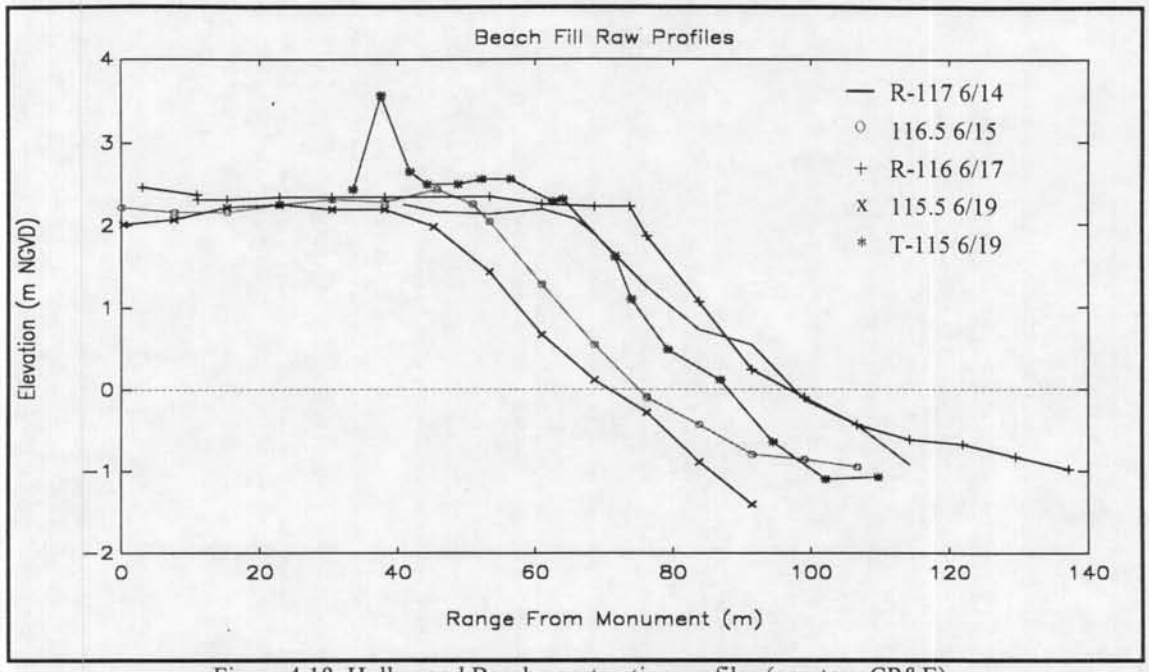

Figure 4.18 Hollywood Beach construction profiles (courtesy CP&E)

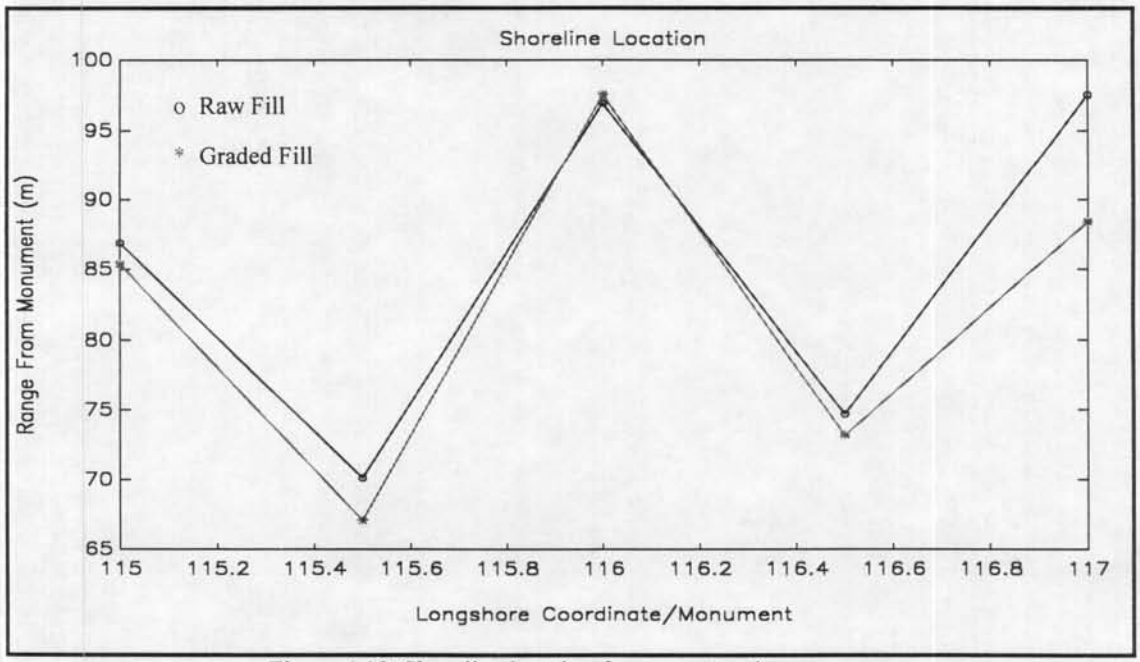

Figure 4.19 Shoreline location from construction surveys

The construction survey data show good agreement with the shoreline positions found from the video data. For example, the survey transect off R-116 shows the water line to be around 96 m from the monument. The water line is taken at 0 NGVD. A corresponding image transect, measured from video data at R-116 on June 17, shows the shoreline at 95 m from the monument. Image transects were taken with Global Lab Image profile tool. The profile tool plots non-dimensional pixel intensity along any line drawn on the image. Image water level is taken as the horizontal location where the intensity abruptly changes value due to the intersection of water and sand. The presence of a shorebreak eases this process, since it causes a bright band along the shoreline. Frequently there will be a series of intensity peaks and valleys along the beach face (of the rectified image), due to variations of sand moisture content and seaweed lines. The computer operator can visually asses the image to resolve ambiguities in the intensity profile and successfully select the shoreline.

The transect at R-116 has the best correlation of the transects selected, due to the convenience of the image baseline set parallel to the east-west ground coordinate of R-116. The image baseline runs parallel to the west end of the broadwalk on Hollywood Beach (about N 5° E) and passes through R-116. In order to check the shoreline position at the other monuments, the survey data must be adjusted to the image baseline. Table 4.1 presents the results of the transects measured from the images. Monuments R-117 and T- 115 have reduced accuracy, since they lie just outside the effective video window."

Table 4.1 Shoreline position comparison

Monument	Survey Date	Shoreline Pos. (m) From Survey Data	Shoreline Pos. (m) Adjusted to Images	Shoreline Pos. (m) From Image Data	Error (m)
T-115	6/19/91	86	-	80	-6
115.5	6/19/91	69	79	82	3
R-116	6/17/91	96	-	95	-1
116.5	6/15/91	75	83	79	-4
R-117	6/14/91	92	77	80	3

The RMS difference between the image based estimates and the survey based estimates is 3.77 m horizontally. As stated previously, the image data profiles do not have the influences of tides or swash action removed. Also, the problem of considering differences between "mean water level" and "NGVD" can effectively reduce accuracy. According to the NOAA Datum Division, Mean Lower Low Water for Haulover Pier (nearest site to Hollywood Beach) is 0.28 m below NGVD. From tidal data in mid-June 1991, the mean water level was calculated to be 0.297 m above MLLW. Therefore, the observed mean water level should be less than 2 cm above NGVD.

A more detailed study would need to be performed to get precise results; however, the image measurement technique looks at the horizontal position of the shoreline, over a large spatial area. This position can fluctuate depending on the beach slope, tide, and wave conditions. As an example, the average beach fill slope is considered. From the profile data, the average beach face slope of the raw profiles is around 0.097 and the graded slope is around 0.076, averaging to 0.087. The average tidal range for mid-June 1991 was around 2.5 feet. As a worst case scenario, three feet vertical on a slope of 0.087 becomes 34 feet or roughly 10 m in the horizontal. With this information, the errors resulting from image-based estimates are within the range of the tidal influence.

The maximum resolution of the video technique (in this case) is limited to 1 m in any direction, since the images are rectified to 1 m/pixel. The dominant advantage to the video technique is the large spatial scale and the flexible temporal scale at which such information can be extracted. If a particular subject was under study, the VMS setup and image analysis could be tailored for the specific problem. For example, the images could be rectified at 0.5 m/pixel for a more detailed result.

4.3.2 Bars and Surf Zone Width

Sand bar morphology is important to coastal engineers and scientists because the understanding of them is imperative to a total assessment of nearshore hydrodynamics and sediment transport. The study of bars and surf zone width with video monitoring

techniques has been investigated by Dr. Robert Holman's group at Oregon State University. The highlights of their intensive research were presented in Section 1.4. In this paper, a similar technique is implemented for completeness of the video monitoring subject matter.

The Miami Beach VMS deployment included the time averaging scheme as outlined in Section 2.2.2. Selected scenes were digitized 10 times over 5 minutes (10 frames per scene) and digitally added together for a time average. The resulting images reveal the areas of wave dissipation and the bar location, due to the preferential breaking of waves over the sand bar (Lippmann and Holman, 1987). The shoreline is also enhanced by the persistent shorebreak. This technique also removes the effect of the swash, since we average over multiple wave periods. Figure 4.20 presents an image from the Miami Beach deployment, taken on December 20, 1992. The shoreline is indicated by the white band which corresponds to the shorebreak, and the offshore bar is clearly visible with rhythmic characteristics. Some nearshore turbidity plumes are also present in the upper left corner of the view. The heaviest wave dissipation areas clearly indicate the bar location, but the areas of less frequent wave breaking or reforming (shoreward of the bar) are apparent in the nearshore foreground. Use of a longer period of averaging or a larger number of averaged images would eliminate the small amount of noise present, but these "secondary" breaking zones may be of some interest and would not be visible in a true time exposure.

The Miami Beach VMS data set is large and more difficult to review than Hollywood Beach since the images are all digital. A sampling of the time averages were examined and selected for the basic results presented. Figure 4.21 includes a series of rectified images spanning the period between December 1992 and May 1993. Dates are marked in the upper right corner of each image. All images are rectified at 1 m/pixel. Qualitatively, the bar began with crescentic segments in late December. The bar retained

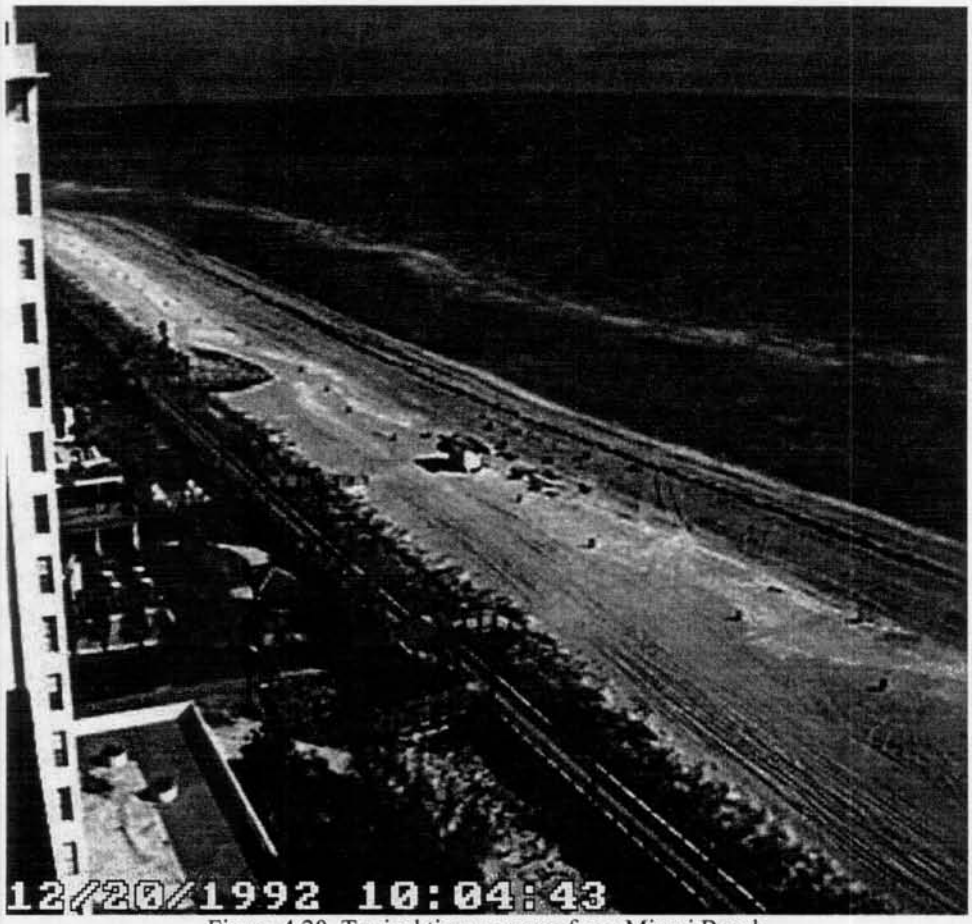

Figure 4.20 Typical time average from Miami Beach

a cross shore width of 30 to 45 m through the series. In early January, the bar seems to have straightened considerably. Both of the previous images were collected during relatively larger wave conditions, since the bar is well-defined. By January 22, the bar has returned to its characteristic crescent shape. The bar definition is less due to smaller incident waves and could be improved with a larger number of averaged frames. The shape of the bar is also described in Section 4.4.1.2, rip currents, as rips are documented on January 23 at the longshore locations which correspond to the offshore extents of the crescentic bar segments.

The months of February and April were characterized by extended periods of little wave activity. If the incident waves do not break over the bar (indicating a small incident

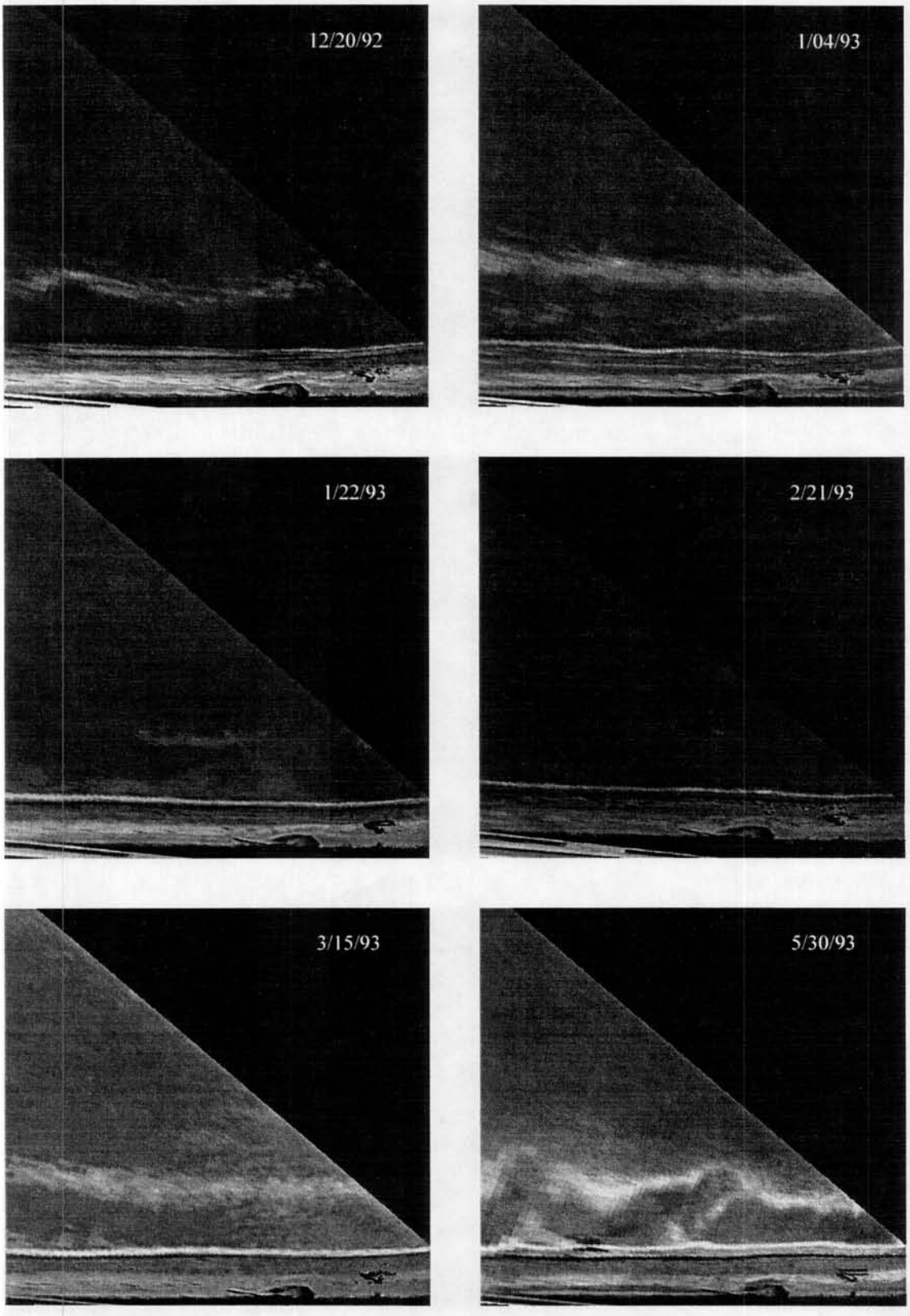

Figure 4.21 Miami Beach bar progression

wave height), then the time average technique provides no additional information about the bar. This is a drawback of the technique, but little wave activity generally implies a minimal amount of sediment transport and bar movement.

On March 15, the bar again has taken its characteristic shape, with a slight shoreward dip in the middle of the image. May 30 provides an interesting scene, where a persistent southeast wind had generated some good-sized waves. The curved pattern may be due to rip currents or a wave reforming and breaking process. According to Lippmann and Holman (1989), a combination of high waves and wind has a tendency to increase the errors associated with the cross shore location of the bar. Under these conditions, unexpected results may occur as foam may be blown shoreward of the dissipation zone, effectively weighting the bar location landward.

In order to illustrate the general concept of the quantitative aspects which result from the time averaging technique, a cross shore intensity profile is taken with the use of an image processing system. Figure 4.22 presents the intensity plot and corresponding surveyed beach profile which were taken at the same longshore coordinate on Miami Beach, just south of 25th Street. The survey profile was performed on December 12, 1992, and the intensity plot was taken from an image on December 20. Beach profiles were only taken on two occasions, December 12, 1992 and January 14, 1993, both during periods of little wave activity. A general comparison can be made since little wave activity occurred until December 17, so only small sandbar movement was expected. Both transects were taken near mid-tide, at similar water levels.

The intensity plot in Figure 4.22 is non-dimensional, so only relative values on the y-axis are used. The apparent correlation of the magnitude of the survey and intensity profiles is pure coincidence. The intensity profile magnitude was scaled to fit the range of the survey profile. Intensity peaks correspond to brighter areas of the image, including wave dissipation zones. Moving from left to right, a series of peaks and troughs along

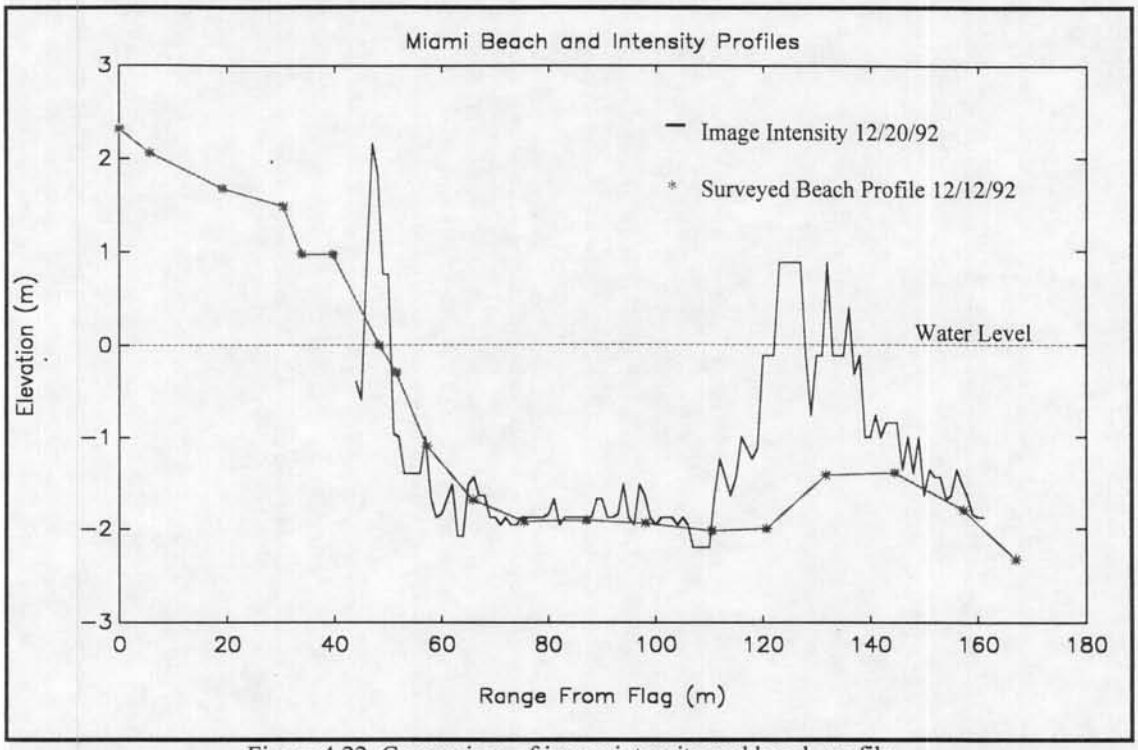

Figure 4.22 Comparison of image intensity and beach profile

the berm and foreshore due to onshore objects (like vegetation and high tide seaweed lines) has been omitted for clarity. The intensity maxima around range 50 m corresponds to the shorebreak, and correlates well with the location of sea level on the beach profile. An area of relative darkness (range 55 m to 115 m) corresponds to the trough area and little or no wave breaking. The offshore bar is apparent on both the intensity and beach profiles. The landward skewing effect of the bar crest by around 10 m is evident, probably due to the persistence of foam in the trough area (Lippmann and Holman, 1989). The overall width of the bar is consistent for both the image intensity and the beach profile, around 45 m. Similar profiles could be taken at various intervals along the images to determine the bar location, width, and surf zone width spatially and temporally.

Overall, the time averaging technique is effective for the qualitative asessment of sand bar morphology, as well as some general quantitative analysis. Particular attention must be paid to the local weather conditions as they are not as obvious in the time

averages as in instantaneous images, and it has been shown that the conditions can affect the results of the time averaging technique.

4.4 Turbidity Phenomena

According to Dompe (1993), turbidity is defined as a measure of the reduction in the clarity of water due to the scattering and absorption of light by suspended particles. Many factors account for differing levels of coastal turbidity, including particle concentration and physical characteristics. The particles which make up turbid water may include sand, silts, clays, and any variety of microscopic organisms or organic matter.

The great concern over turbidity levels in the coastal environment stems from the fact that increased levels of turbidity, due to natural or man-induced events, are detrimental to some benthic communities. During the Hollywood Beach renourishment of summer 1991, in-situ instrumentation was deployed for a comprehensive turbidity study, which included the causes and effects of fluctuating turbidity levels (Dompe, 1993). The instrument packages recorded data at two specific sites in 5 and 10 meter depth. The video data from Hollywood Beach provides the ability to see the spatial variations in turbidity patterns. The current goal is to map the turbidity patterns to increase understanding of turbidity motion and its forcing mechanisms in the coastal environment. Turbidity phenomena have been grouped into two categories for this study. Readers should remember that although natural and man-induced turbidity phenomena are categorized independently, they are not mutually exclusive events.

4.4.1 Natural Turbidity Structures

Natural turbidity structures, as pertinent to this paper, are defined as organized and well described patterns of elevated turbidity which result from natural events. These natural forcing events include, but are not limited to, wave activity, currents, wind, and tides. Besides the normal background turbidity levels of any location and time, two regularly occurring turbidity features are classified as natural: lobes and rip currents.

4.4.1.1 Lobes

Natural turbidity is always present as so called "background" turbidity, qualitatively estimated by the "cloudiness" of the water and quantitatively measured in Nephelometric Turbidity Units (NTU). A visual distinction is possible in the relatively clear water of Hollywood Beach, which is labeled class 3 water (extending from Jupiter Inlet to the Dry Tortugas). The video data from Hollywood Beach contains unique events that document the propagation of turbidity fronts, made possible by the clarity of the coastal waters. These events produce turbidity patterns of a finger- or lobe-like structure, hereafter termed turbidity lobes.

Although many such events occur throughout the video data set, two of the most dramatic are presented here. The first occurred on April 26, 1991, which was only two days after the beach renourishment had begun (several miles south). Figure 4.23 presents the rectified views of the lobe progressions which occurred between 3 PM and 6 PM. The letters in the upper right of each image correspond to the plots in Figure 4.24. Figure 4.24 contains a graphical representation of the progression, including the mean shoreline and dominant areas of wave breaking for April 26. The wave breaking zones were taken as an average for the images used.

At 2:51 there is the persistent nearshore turbidity that extends to 188 m offshore. This longshore band of turbidity is present under typical conditions at Hollywood Beach and usually extends beyond the surf zone, to a depth around 6 m (20 ft). From profile data at Hollywood Beach, this distance from shore corresponds to a somewhat steeper area of the profile, offshore of the outside bar, where the depth drops from about 3 m to 6 m. The persistent band of turbidity remains during periods of relatively small wave action, seemingly forced by offshore-directed circulation and diffusion until the energy levels decrease to allow particle settling.

At 3:51 three distinct lobes form with longshore spacings of 320 m to the north and 280 m to the south. A shorebreak is distinctly visible along the shoreline, and the

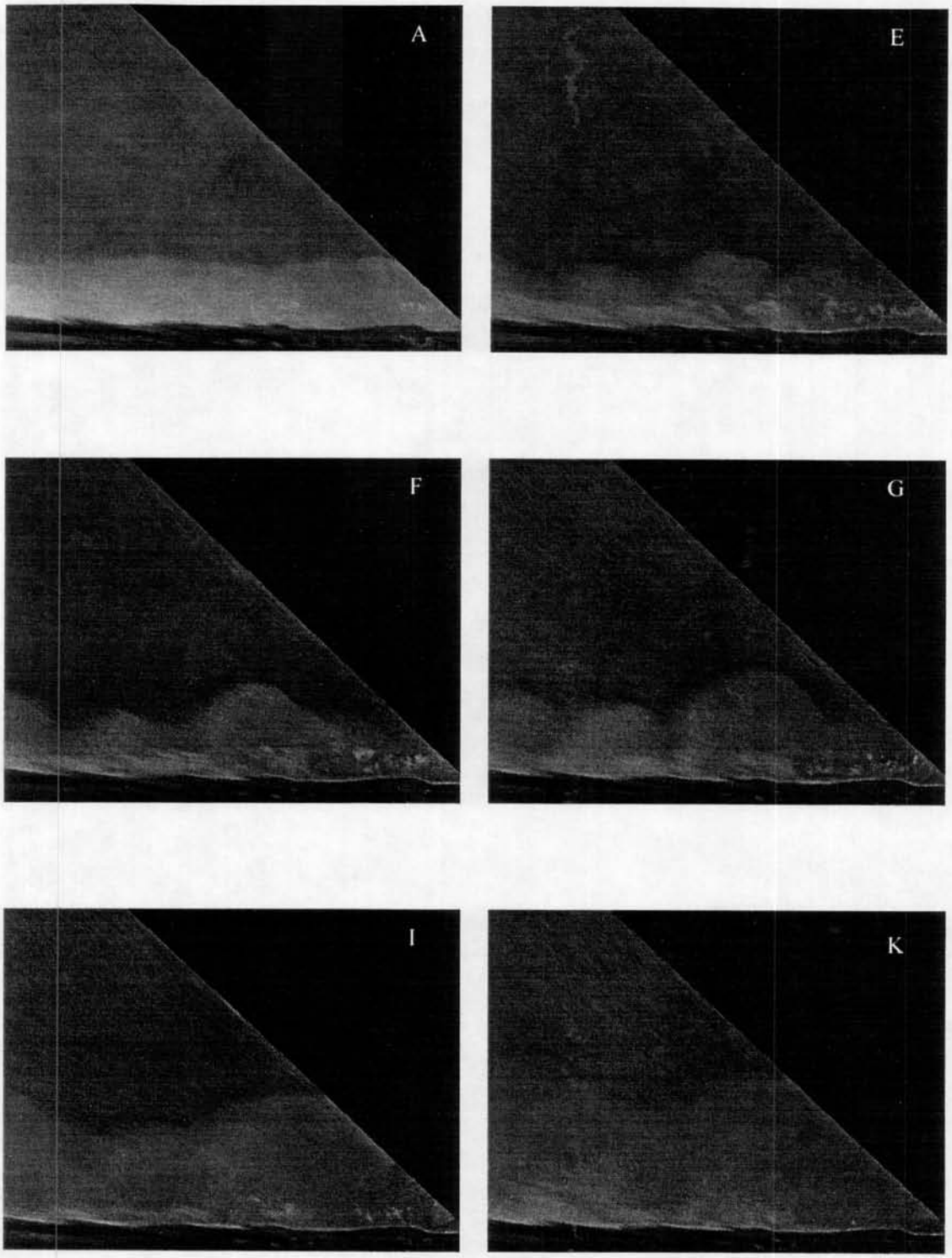

Figure 4.23 Turbidity lobes propagation, April 26, 1991

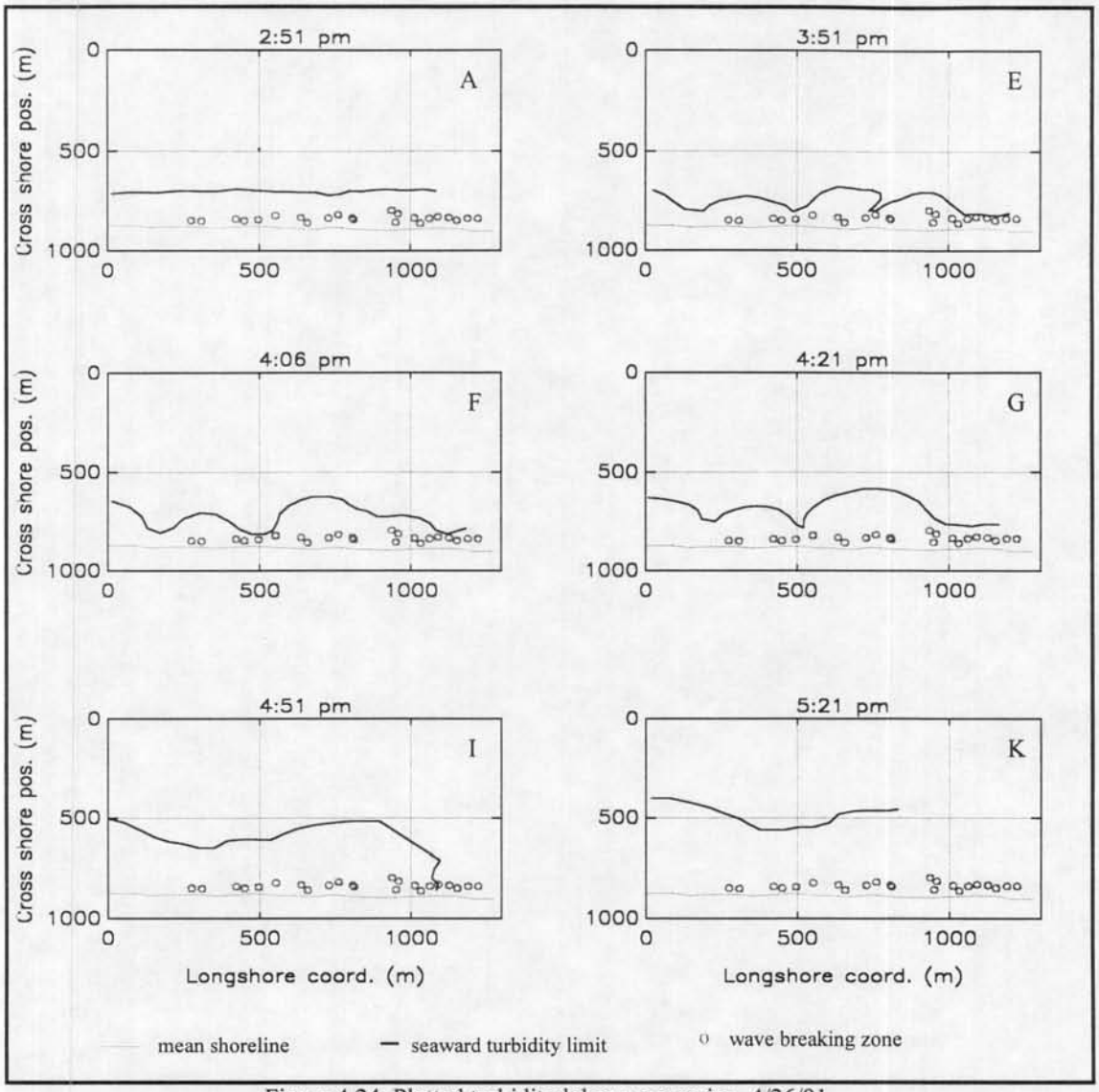

Figure 4.24 Plotted turbidity lobes progression, 4/26/91

waves tend to be concentrated on the "bumps" (shoreline deviations from a straight beach) along the shoreline. The offshore turbidity lobe peaks occur offshore of the concentrations of breaking waves. The turbidity lobes propagate eastward while the central and south plumes merge by 4:06 PM. By this time the visible lobe tips are separated by about 396 m. The northmost plume is visible but difficult to measure since it extends north off the view. The surf zone appears wider during the middle frames of the six shown. From 4:51 through 5:21 PM, the lobes continue offshore until they merge

become less distinct. The waves decrease and the northern lobes overtake the southern lobe.

Table 4.2 presents the results from an analysis of the image data. The seaward extent of each feature was identified and recorded by an operator with the aid of an image processing system. Pertinent displacements alongshore (dy, + southward), cross shore (dx, + offshore), and absolute (dz), elapsed time (dt), as well as corresponding velocities are calculated and tabulated.

To be complete in the data presentation, Tables 4.3 and 4.4 present the in-situ data from the instrument packages and the wind from Miami International Airport from April 26, 1991. The data in Table 4.3 were taken on the inner site at Hollywood Beach, which is about 300 m offshore of Broward T-115, and the outer site, which is about 0.5 miles southeast of the inner site. Positive values of U and V, in-situ current velocities, are onshore and longshore down the coast (southerly). Wave direction Θ is denoted with standard compass headings. NTU turbidity values were measured 0.77 m from the sea bed for the inner site, and 0.45 m for the outer site. The tide values shown in Table 4.4 were taken from *Tidemaster*, a commercial tide prediction software package.

Table 4.2 Data summary of turbidity lobes, April 26, 1991

Images	dt (s)	dx (m)	dy (m)	dz (m)	Vx (m/s)	Vy (m/s)	Vz (m/s)
North Plume							
E-F	900	16	-22	27	0.018	-0.024	0.03
F-G	900	36	38	52	0.04	0.042	0.058
G-I	1800	68	86	110	0.038	0.048	0.061
I-K	1800	64	32	72	0.036	0.018	0.04
Averages					0.033	0.036	0.047
South Plume							
E-F	900	58	54	79	0.064	0.06	0.088
F-G	900	40	42	58	0.044	0.047	0.064
G-I	1800	64	118	134	0.036	0.066	0.075
I-K	1800	62	58	85	0.034	0.032	0.047
Averages					0.045	0.051	0.069

Table 4.3 In-situ data summary, April 26, 1991

Site	Inner (5 m depth)		Outer (10 m depth)	
Time	12:00 PM	4:00 PM	12:00 PM	4:00 PM
Hs (m)	0.2548	0.5596	0.2441	0.5599
Θ	-	83.571	-	-
Tp (s)	2.48	3.71	3.16	3.82
U (m/s)	0.0468	0.0541	0.03107	-0.02382
V (m/s)	-0.0713	0.126	-0.03096	0.06348
NTU	0.88	0.914	1.02	1.07
Tides	Time	Elevation (ft)		
High	8:11 AM	2.3		
Low	2:32 PM	-0.2		

Table 4.4 Wind data from April 26, 1991

Time	Direction	Speed (kts)
11:00 AM	160	12
12:00 PM	180	12
1:00 PM	140	17
2:00 PM	140	16
3:00 PM	140	8
4:00 PM	90	5
5:00 PM	140	5
6:00 PM	140	7

The turbidity lobes of April 26 propagate offshore with an average velocity of 0.033 m/s and 0.045 m/s for the north and south plumes, respectively. The magnitude of the cross shore lobe speed is similar to the in-situ cross shore current speed of about 0.05 m/s. However, the direction of the measured current is onshore. Because the sensor is in the lower portion of the water column, this suggests a two-dimensional cross shore circulation pattern with onshore flow near the seabed and offshore flow near the surface.

The wave direction is from the northeast, which corresponds to the southward propagation of the lobes. The measured longshore current velocity (0.126 m/s) is in agreement in direction but about three times the speed of the longshore lobe propagation. The tide is incoming throughout the propagation and the afternoon sea breeze phenomenon is in effect, as evidenced by the wind data. The east coast of Florida

undergoes typical sea breeze conditions during the summer months. This activity is characterized by a clockwise cycle of winds that begin light and peak in the mid afternoon. This wind forcing causes changes in the wave and current conditions that are superimposed on the normal tidal conditions.

Turbidity readings from the in-situ instruments show no evidence of the lobes. There are two likely explanations for this. First, the measurements are made close to the bottom of the water column, and the observed turbidity is on (or near) the surface. Second, turbidity levels increase between noon and 4 PM, but the level is low (0.9 NTU) and no reading is made around 5 PM when the lobes reach the area of the inner instrument site. Determination of the vertical distribution of turbidity is not directly possible with video images and requires a more intensive study.

The other good example of turbidity lobes occurred on May 24, 1991. This set of 3 lobes is perhaps the most dramatic event recorded with the VMS. The lobes propagate between 11:30 AM and 1:30 PM. After a period of inactivity, a second wave of plumes forms. Figure 4.25 presents the progression images, and Figure 4.26 shows the plotted plume boundaries with the mean shoreline location and areas of dominant wave breaking.

As in the previous example, the first image has relatively low wave activity accompanied by a uniform longshore turbidity band. A perturbation in the turbidity band at 10:57 leads to the formation of lobes by 11:28. By noon, the lobes are well-defined, quite symmetric, and spaced about 400 m longshore. Here, the waves appear larger and the width of the surf zone is around 85 m. The areas of concentrated wave breaking provide suspension in the surf zone. The lobe feeder zones occur between areas of concentrated wave breaking, around x = 500 and x = 800 in Figure 4.26.

At 12:16 PM the two lobes have moved offshore and south, with a velocity around 0.1 m/s. Their spacing is still about 400 m, as they are moving together. A third plume comes into view from the North. By 12:48 PM, the original two lobes have

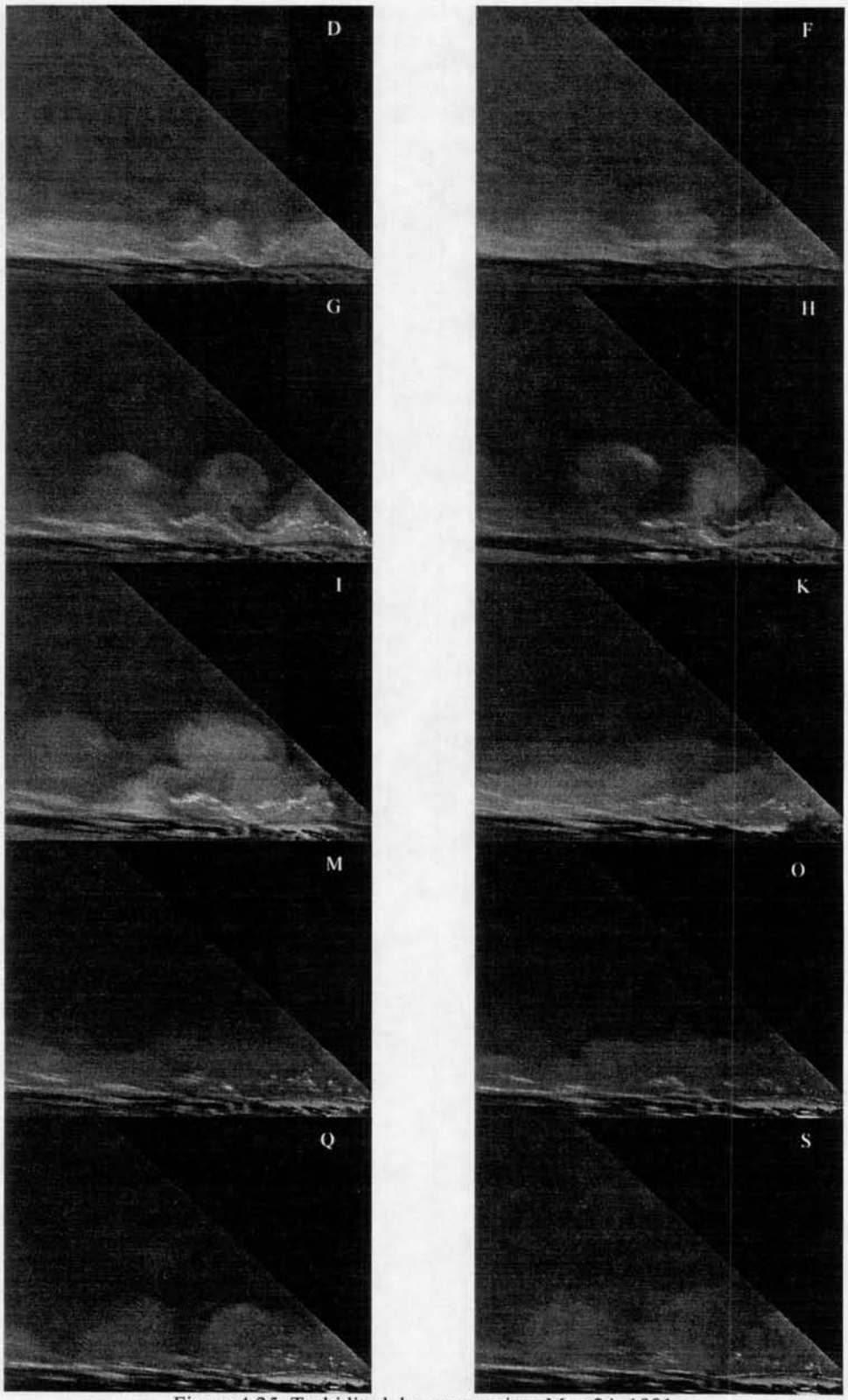

Figure 4.25 Turbidity lobe progression, May 24, 1991

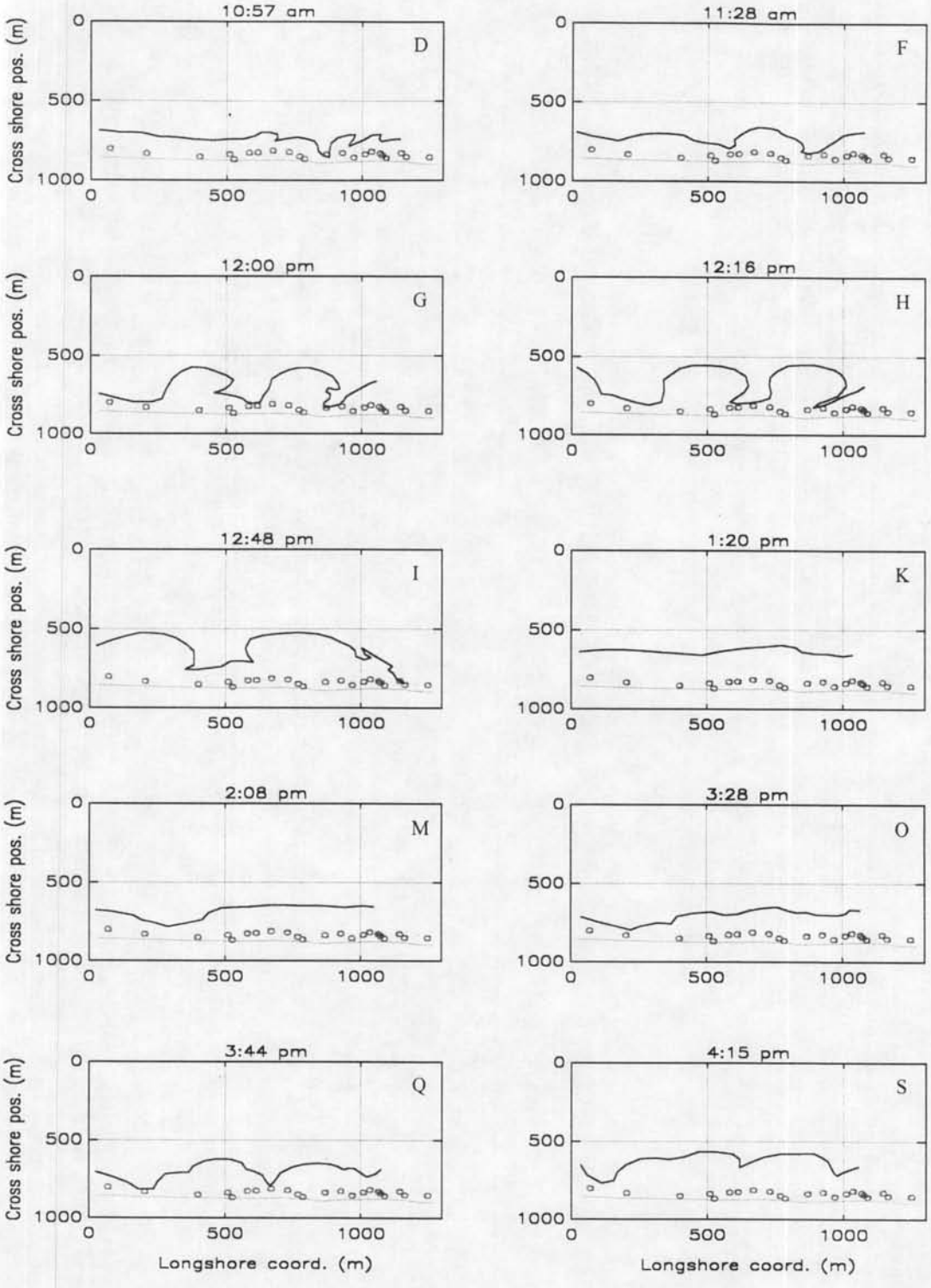

Figure 4.26 Plotted turbidity lobes progression, 5/24/91

merged into one (between x = 500 and 1000 in Figure 4.26) and the north lobe has moved into the left of the view. The offshore tips of the turbidity lobes reach to around 4.5 times the width of the surf zone.

From 1:20 PM through 3:28 PM, the lobes disperse and the uniform turbidity band reforms out to around 240 m offshore. This occurs at low tide, when the surf zone width decreases to 75 m. The turbidity band has various perturbations, but no well-defined "bumps."

After 3:28 PM the lobes reform in similar locations to the earlier ones. Their separation is about 360 m at 3:44 PM. These lobes, though not as dramatic as the earlier set, propagate in a similar fashion toward the southeast. Their velocity is somewhat lower, slowing from about 0.08 m/s to 0.04 m/s.

Table 4.5 presents a summary of the information gathered from image data on May 24, 1991. Quantities shown in each column are as defined previously, with the addition of the column on the far right, W, which is the change in width of the lobe at y = 330 pixels. This arbitrary location is about 217 m from the mean shoreline. The corresponding in-situ instrument and tide data are listed in Table 4.6. Miami International Airport wind readings are presented in Table 4.7.

Table 4.5 Data summary of turbidity lobes, May 24, 1991

Images	dt (s)	dx (m)	dy (m)	dz (m)	Vx (m/s)	Vy (m/s)	Vz (m/s)	W (m)
North Plume								
D-F	1920	-	-	-	-	-	-	-
F-G	1920	126	70	144	0.066	0.036	0.075	-
G-H	960	32	100	105	0.033	0.104	0.109	64
H-I	1920	28	272	273	0.015	0.142	0.142	100
O-Q	960	8	90	90	0.008	0.094	0.094	-
Q-S	1920	-78	-22	81	-0.041	-0.011	0.042	-
Averages					0.033	0.077	0.092	-
South Plume								
D-F	1920	38	48	61	0.02	0.025	0.032	-
F-G	1920	78	98	125	0.041	0.051	0.065	126
G-H	960	30	84	89	0.031	0.088	0.093	60
H-I	1920	-	-	-	-	-	-	-
O-Q	960	64	30	71	0.067	0.031	0.074	-
Q-S	1920	62	34	71	0.032	0.018	0.042	-
Averages					0.038	0.043	0.061	-

Table 4.6 In-situ data summary, May 24, 1991

Site	Inner (5 m depth)	
Time	12:00 PM	4:00 PM
Hs (m)	0.3858	0.5534
Θ	115.714	115.714
Tp (s)	3.41	3.707
U (m/s)	0.0574	0.0445
V (m/s)	0.1653	0.0402
NTU	11.24	11.08
Tides	Time	Elevation (ft)
High	6:54 AM	2.1
Low	1:20 PM	-0.1

Table 4.7 Wind data from May 24, 1991

Time	Direction	Speed (kts)
10:00 AM	110	9
11:00 AM	110	15
12:00 PM	100	14
1:00 PM	100	8
2:00 PM	100	12
3:00 PM	110	15
4:00 PM	80	13
5:00 PM	110	13
6:00 PM	110	14

Table 4.6 only contains data from the inner instrument site. The outer site was not operational at this time.

An overview of the data presented leads to an inexplicable forcing mechanism. The waves approach from the southeast (115°), residuals of a large storm which occurred between May 19 and 22 (see Figure 4.3). The in-situ cross shore current reading and the offshore average lobe velocity agree as in the previous example, on an order-of-magnitude basis. Despite the wave direction, the in-situ current direction and longshore lobe velocities are both toward the south, which is counter-intuitive. The wind data is also inconclusive, with the speed varying throughout the day and the predominant

direction at 100°. In this case, the tide is dropping during the initial lobe progression (low tide is at 1:20 PM) and rising during the secondary lobe progression.

In each case presented, the dominant forcing mechanisms appear to be the waves and nearshore currents. The increased nearshore sediment suspension, due to wave action, saturates the surf zone and eventually escapes through breaks in the surf zone or rip currents. The offshore and longshore driving forces appear to be related to the advective currents measured in-situ, but specific information about the nearshore circulation (particularly convection) is not known. The effect of the seabreeze on the lobes is somewhat ambiguous, since the wind direction is predominantly opposite to the water surface flow. Initial expectations were that the tidal influences would be more obvious (incoming or outgoing). However, the tidal height during the peaks of both lobe progressions was around 0.1 ft. above MLLW. For the characteristics of this beach, perhaps a certain combination of tidal height and waves triggers the jetting of the turbidity offshore. The importance of the diffusion part of the lobe propagation is difficult to estimate with the nearshore concentration (initial concentration for diffusion analysis) unknown. An intensive study including 3D mapping of the nearshore sea bed, video monitoring, and vertical concentration measurements within the lobes would help to determine the forcing mechanisms of these turbidity lobes.

4.4.1.2 Rip currents

The second category of natural turbidity structures is rip currents. Rip currents are responsible for the transport of potentially large amounts of water and sediment to a region outside the surf zone. They are of importance to the coastal scientist because they greatly influence (or are influenced) by the local sea bottom topography, currents, and wave conditions.

Although the so-called "chicken or the egg" dilemma often arises when rip currents are discussed, there are conditions required for rip current formation. A barred bottom

with quasi-periodic spacing is generally accepted as a rip current scenario, where incident waves break preferentially over the bars. The longshore variation of wave breaking forces a circulation which is shoreward over the bars and offshore at the rip currents. The rip currents are fed by water flowing alongshore, toward them, from the areas of wave breaking (Fredsoe and Deigaard, 1992). This is the simplest scenario which is complicated considerably with complex bottom topography and irregular waves. At this level the question is not how the rips form, but whether or not they can be recorded with video.

Evidence of rip currents may be assumed from the results of Section 4.4.1.1 (as mechanisms for forcing turbidity lobes), but the highest quality images of rip currents were obtained in Miami Beach on January 23, 1993. Figures 4.27 and 4.28 present a progression of a rip current which formed between 11 AM and 12 PM on January 23. At the center of the images, the breaking waves are seen to be from the southeast. Figure 4.29 is an oblique time average of the scene, taken at 12:06 PM. The crescentic bar pattern is revealed with the time averaged image. The rip forms at the horns of the crescentic bar segments, where the bottom contours permit a return flow.

In Figure 4.27 at 12:00, the rip current has the traditional shape with a narrow channel (about 20 m width) inside the surf zone and a mushroom-shaped head which extends to 115 m offshore. The spacing to the next rip to the north is about 355 m. The waves breaking over the bar near the center of the image are 75 m offshore, and the waves which flank the rip head are 85 m offshore.

In Figure 4.28 at 1:00 PM, the rip current is somewhat more diffuse. It extends to 155 m offshore and is characterized by a northward hook outside the surf zone. In both images, the sediment feed zone for the rip current is apparent just to the north of the shoreward end of the rip. The offshore hook to the north and the rip current skew to the north are in agreement with the incoming wave direction.

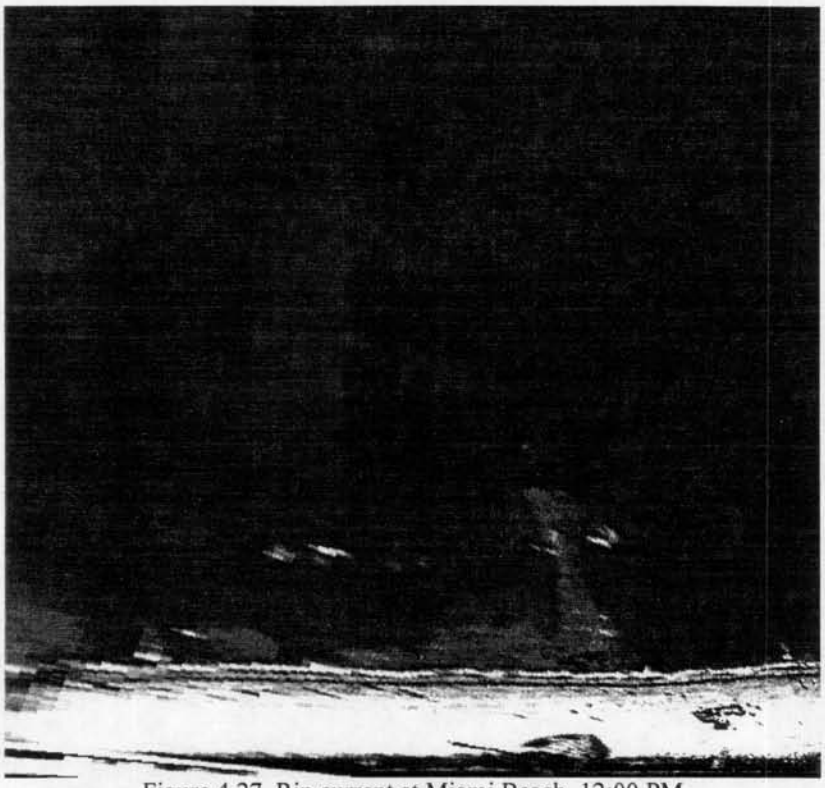

Figure 4.27 Rip current at Miami Beach, 12:00 PM

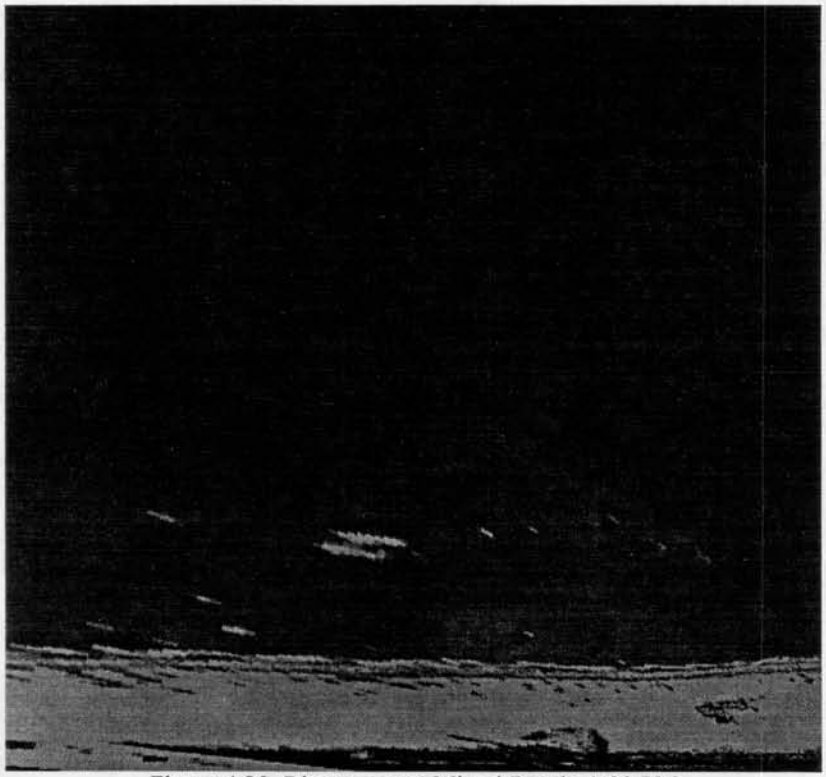

Figure 4.28 Rip current at Miami Beach, 1:00 PM

Figure 4.29 Time averaged image, Miami Beach

The further study of rip current geometry and frequency is ideally suited to video monitoring. By implementing a higher frequency sampling scheme, the formation of such rips can be documented in great detail. Rips can be identified from time lapse video records in areas where swimmer safety is important, as in Florida, where rips often take unsuspecting tourists by surprise. The video technique may also provide the ability to assess the local waves and nearshore features which dictate rip current characteristics.

4.4.2 Man-Induced Turbidity Structures

The second category of turbidity structures results from man-induced events. For this study, we consider dredge and fill operations during beach nourishment as the primary source of man-induced turbidity. Two direct results from the dredge and fill method are nearshore turbidity snakes, caused by the slurry discharge on the beach, and offshore turbidity snakes that result from hopper dredge overflow.

3.4.2.1 Discharge snakes

The beach nourishment procedure inherently produces turbidity. As shown in Figure 4.4, the dredge discharge is placed at the head of a dike and trough system which runs parallel to the shoreline. In theory, the dike system routes the discharge slurry along the beach, where the sand gets deposited and the water percolates into the beach face and runs into the nearshore region. Unfortunately, the lower quality sediments (finer matter) remain suspended in the water and escape to the nearshore region. This is the cause of what are hereafter referred to as discharge snakes. These discharge snakes have been observed on the Hollywood Beach video data when the nourishment operations were near the camera field of view.

The most dramatic example of a discharge snake occurred on June 12, 1991. According to the dredger's log, the discharge point was located 30.5 m south of Broward County Monument R-118. This point is about 335 m south of the rectified camera view. Figure 4.30 presents a progression of a discharge snake from June 12. Figure 4.31 shows the same sequence, plotted, including a longshore and cross shore scale for reference. Also included are the mean shoreline location for June 12 and areas of dominant wave breaking, as identified in the images. All digitization was done by a computer operator, by first enhancing the image contrast and manually selecting the locations from the images. This technique may be considered primitive, but the non-uniformity of the turbidity patterns makes computer identification almost as subjective as human identification.

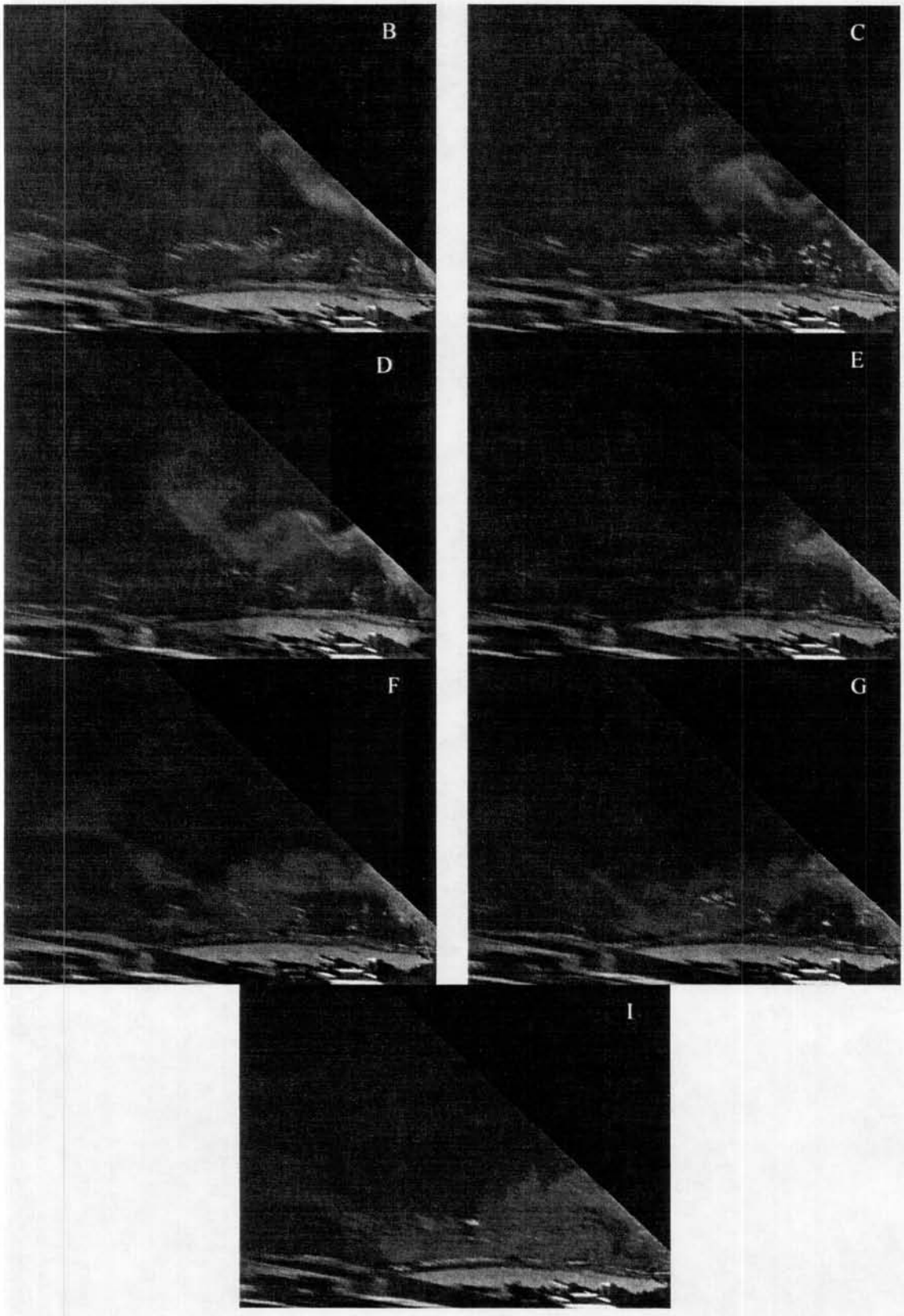

Figure 4.30 Discharge snake progression, 6/12/91

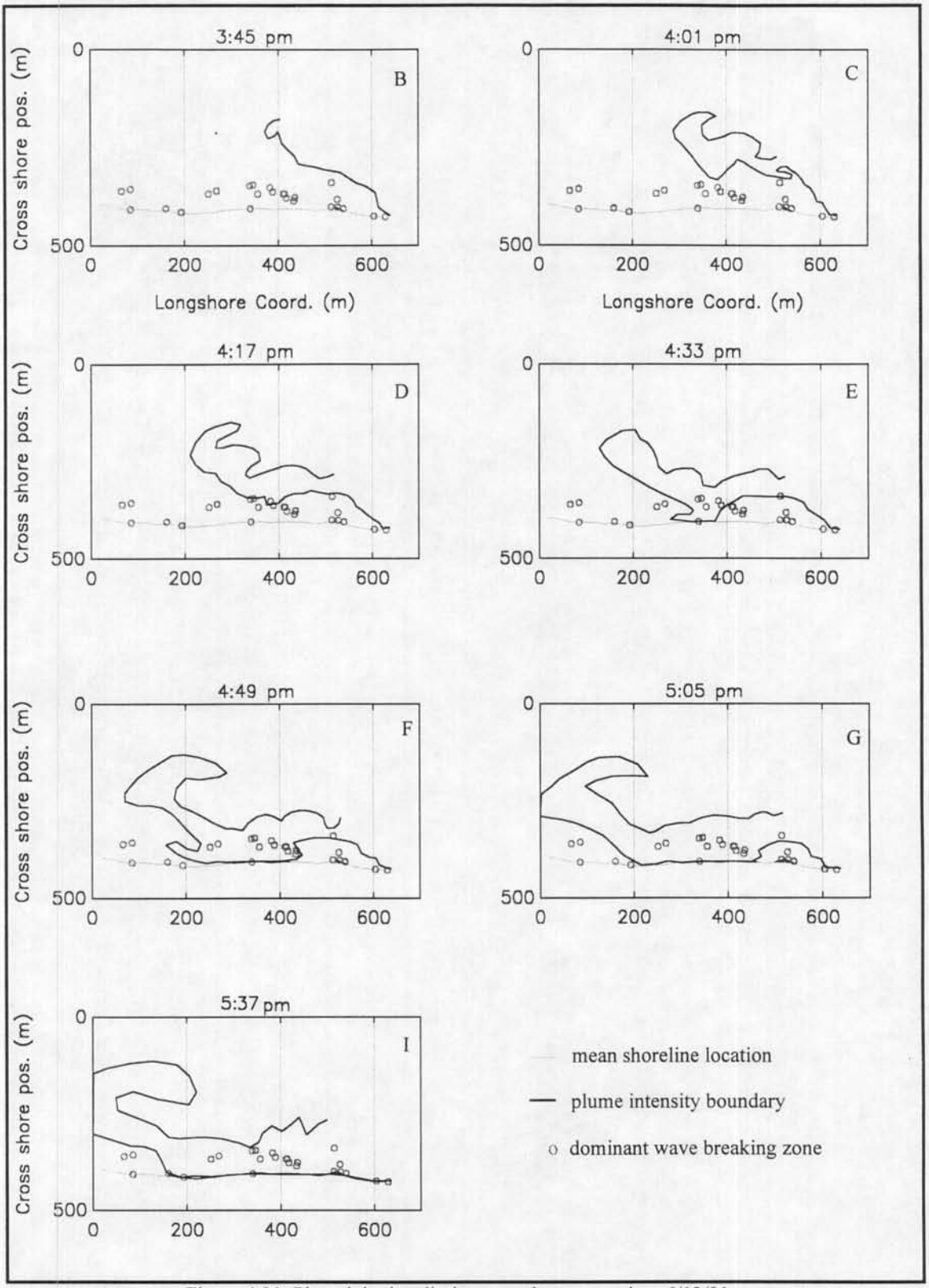

Figure 4.31 Plotted dredge discharge snake progression, 6/12/91

Similar to Holman et al. (1990), a computer routine could be implemented to select an appropriate threshold of intensity (determined by the user on a best fit basis) and search each column of pixels for that location. This would automate the identification process, but would still take operator time and supervision. For our introductory analysis, the manual identification is appropriate, since we are looking for general, large-scale motion of the discharge plumes.

The snake advects generally northward throughout the progression at 0.08 m/s. The cross shore motion of the snake oscillates, but has no significant offshore component. At 3:45 and 4:01 PM the visible turbidity lies outside the surf zone. The shoreward edge of the snake encounters the surf zone at 4:17 (around x = 400, Figure 4.31) and moves toward shore, presumably under the influence of the waves. The offshore reach of the snake hooks southward throughout the progression.

Between 4:33 and 4:49 PM a small lobe nearshore advects northward. During the final two frames, the northern reach of the snake cannot be determined from the data, but the offshore extent remains fairly constant around 265 m. The southern reach of the snake spreads to cover the entire surf zone and extend seaward. Table 4.8 presents a summary of data from an analysis of the images.

Table 4.8 Data summary of discharge snake, June 12, 1991

North Edge of Plume						
Images	dt (s)	dx (m)	dy (m)	dz (m)	Vy (m/s)	Vz (m/s)
B-C	960	3	-84	84	-0.088	0.088
C-D	960	-25	-76	80	-0.079	0.084
D-E	960	17	-83	85	-0.087	0.088
E-F	960	-13	-58	59	-0.06	0.062
F-G	960	-	-	-	-	-
G-I	1920	-	-	-	-	-
Averages					-0.079	0.081
Nearshore Tip						
E-F	960	37	-123	128	-0.128	0.134

In Table 4.8 dx specifies cross shore displacement (positive offshore), dy specifies longshore displacement (positive south), and dz is the absolute displacement. The average velocity in a northerly direction is about 0.08 m/s. The mean offshore reach of the visible turbidity is 262 m offshore and the maximum extent of the snake offshore is 297 m. In images G and I the turbidity snake advects north of the rectified view, so no estimation of position is made.

To help understand the forcing of the snake, reference is made to some of the in-situ instruments and weather data from June 12. Table 4.9 presents a summary of the pertinent in-situ data.

Table 4.9 In-situ data summary, June 12, 1991

Site	Inner (5 m depth)		Outer (10 m depth)	
Time	12:00 PM	4:00 PM	12:00 PM	4:00 PM
Hs (m)	0.4616	0.4231	0.3368	0.3214
Θ	102.86	-	-	-
Tp (s)	3.16	3.6	3.71	3.71
U (m/s)	0.0161	0.0391	0.0361	0.0473
V (m/s)	-0.0252	0.0917	0.0167	0.0153
NTU	16.72	16.59	4.98	5.5
Tides	Time	Elevation (ft)		
High	9:25 AM	2.4		
Low	3:52 PM	-0.7		

Wind data from the Miami International Airport is presented in Table 4.10.

Table 4.10 Wind data from June 12, 1991

Time	Direction	Speed (kts)
11:00 AM	70	12
12:00 PM	80	14
1:00 PM	90	12
2:00 PM	110	10
3:00 PM	80	15
4:00 PM	80	10
5:00 PM	130	11
6:00 PM	100	10

The wave direction, although indeterminate at 4 PM, is from the southeast at noon. This explains the general northward motion of the turbidity snake nearshore. According to in-situ instrumentation, a significant event occurred on June 10 when significant wave height from the northeast exceeded 1 m. This was verified by the fact that dredging was postponed on June 10 due to 4 to 7 ft seas. The waves diminished throughout the following days until June 13. The 4 PM in-situ longshore current velocity is 0.09 m/s, which agrees with the southerly "hook" of the plume offshore extent. It is noteworthy that the plume average velocity is north at 0.08 m/s, which may indicate a tidal gyre motion in the area. The small lobe which occurs between 4:33 and 4:49 PM moves with a longshore velocity of 0.128 m/s. This lobe is within the surf zone.

The turbidity values measured by the in-situ instruments may not be characteristic of the snake. According to the image data, the snake does not reach the inner site. Again, we cannot form any definite conclusions about the settling and vertical distribution of the turbidity from the images. To determine the actual forcing mechanisms of turbidity snakes, an intensive field experiment as described in Section 4.4.1.2 would have to be performed.

4.4.2.2. Dredge overflow

Turbidity can also occur offshore, as a result of the overflow from a hopper dredge operation. As sediment is loaded onto the barge, the water and fine particles are allowed to overflow the barge. This process causes the larger, higher quality sediment to remain in the slurry that is deposited on the beach. The consequence of this operation is the resultant turbidity plume that propagates away from the borrow site by advection and diffusion (Dompe, 1993).

Resultant dredge overflow plumes are clearly visible in the offshore region of the Hollywood Beach video data. Unfortunately, the borrow areas were south of the camera views. Overflow plumes are only visible when they propagate northward. Viewing a video time lapse allows a general idea of the propagation time scale, but detailed

measurements are difficult due to the distance from the camera. Figure 4.32 is an example of an image from Hollywood Beach which includes a dredge overflow turbidity plume near the horizon line. This phenomenon has been studied in substantial detail, but could be visually monitored with the VMS. Goodwin and Michaelis (1984) present a comprehensive summary of turbidity plumes generated by a variety of dredge and discharge configurations used in Tampa Bay, Florida.

Figure 4.32 Dredge overflow turbidity plume

CHAPTER 5
CONCLUSIONS AND RECOMMENDATIONS

5.1 General Conclusions

The primary objective of this study was to evaluate the feasibility of utilizing video monitoring for coastal engineering purposes, as an alternative and addition to traditional measurement techniques. This was accomplished with a brief literature review of the published work to date, an introduction to digital image concepts and analysis, and some examples of the applications of video monitoring for coastal engineering.

In a qualitative sense, basic video monitoring has proven to be an excellent method of observing long-term processes (like shoreline position and coastal feature change). Shorter-term observations including sea conditions, weather, and beach use are monitored with a modification of the sampling scheme for higher frequency.

Measurement techniques which result from analysis of video images are in need of some refinement, and even full development in some cases. The measurement of swash motions (Holman et al., 1990) and sandbar morphology (Lippmann and Holman, 1989) has been intensively studied, the latter using a time averaging technique. Time averaging allows for submerged feature and water level determination. The present experiments have shown that shoreline position and general feature length scales are within 5% of surveyed data. Bar crest determination is generally skewed shoreward due to intensity weighting by foam in the profile trough, but the overall bar width is preserved. The technique fails during periods of low wave activity (for submerged feature identification), but this is not regarded as a significant limitation.

The mapping of turbidity phenomena is of current interest due to a growing concern for benthic communities near beach nourishment projects. Turbidity lobes,

discharge plumes, and rip currents are all events which may be responsible for transport of potentially large amounts of water and sediments in the nearshore (and offshore) zones. Some new findings during this study have shown the turbidity plumes at Hollywood Beach to propagate well outside the surf zone (exceeding 3 times the surf zone width) and form under relatively low wave conditions. The longshore separation between plumes averages around 5 times the surf zone width. The forcing of such events is positively linked to waves and currents nearshore, but detailed process descriptions could not be made with the in-situ data recorded. Propagation velocities of the turbidity plumes agree with in-situ current data collected on an order of magnitude basis. The influence of tides and wind is inconclusive from this study. The video data has been used to supplement in-situ instrumentation readings (Dompe, 1993). The complexity of nearshore hydrodynamics requires a more intensive study than performed during this experiment. Quantification of turbidity levels from video data was not addressed due to the complexity of required image analysis, which extends beyond our current capabilities.

Pertaining to the data and techniques used in this report, general benefits and drawbacks of the video monitoring presented can be summarized. Drawbacks can be categorized as logistics or applications. Application drawbacks are threefold. First is determination of the vantage point location, which depends on accuracy of ground surveys. Second, there is a limited ability to perform vertical measurements like wave height. Vertical measurements can be done with advanced photogrammetry but are not part of current research . The third application drawback is the limit on horizontal accuracy. The photogrammetry relates image locations to world distances. Errors in measurements increase with distance from the camera, due to the nature of the technique and resolution of typical digital images. Regardless of this condition, errors in image-based measurements normalized by the distance from the camera are consistently less than 5%. The resolution of the camera, frame grabber, and computer display each affect the measurement capabilities. An optimal scenario contains high resolution equipment

located as close to the desired study area as possible. The desired measurement resolution should be known first, then the appropriate equipment and setup selected to perform any particular study. Logistical drawbacks are also threefold. First, the VMS requires power and a phone line to transmit images. Second, protection against the environment is essential to outdoor deployments. The final disadvantage is the inability to record data at night, unless artificial light is introduced or a low-light camera is employed.

The value of video monitoring has been shown. Cost, versatility, and flexibility are all additional benefits. The cost of a basic Erdman VMS is currently around $15,000. Each study requires individual assessment, but the logistics of deployment and measurement cost far less than a similar study with aerial photographs, survey crew, or field instrumentation packages. This fact alone makes the development of video measurement techniques an attractive option. Versatility is inherent in the many applications of the VMS, which are not limited to coastal engineering. The pinnacle feature of the VMS is the large spatial scale which can be covered with a single image. The flexibility of the VMS allows it to be adapted to any scenario. Here, the benefit is the temporal variability. Any sampling frequency can be set to the needs of the experiment. Images can be sampled every second, hour, day, as dictated by the application. Tape records (burst samples) can be used instead of instantaneous images, and various image processing functions can be employed as necessary. Other benefits include ease of digitization for use and analysis using computers, as well as electronic transmission of data over telephone lines.

5.2 Future Developments

Current research includes the Longboat Key, FL, beach nourishment, where independent measures of turbidity and sedimentation rates are being correlated with beach nourishment. Not only is spatial mapping of turbidity plumes of interest, but also a

method of quantifying turbidity from video data. Problems result when intensity values are extracted from monochrome images, since lighting and camera aperture settings greatly influence the images. To quantify turbidity levels, a standardized method of data collection and calibration (including ambient light levels) and color image analysis techniques would need development.

Determination of the forcing mechanisms of coastal turbidity requires a much more intensive study than that performed in Hollywood Beach, 1991. A spatial array of in-situ instrumentation for measuring waves, currents, and turbidity, as well as three-dimensional seabed plots would be required. The tidal influence on turbidity lobe formation needs further investigation. The idea of a certain tidal elevation, coupled with adequate wave activity, saturating the surf zone with turbidity and then jetting it offshore may be tested with a more intensive study. Also, a sampling of turbidity levels on an event-by-event basis of observed plumes (in a vertical array) would increase an understanding of the vertical distribution of turbidity plumes.

The development of new processing and analysis techniques may reveal improved measurement methods. Use of high resolution cameras and frame grabbers would increase measurement accuracy. Improvements to the rectification program would include a better method of remapping intensity (with interpolation methods, for example, instead of the nearest neighbor technique) and an option to include image information in the black-out area caused by the limit of the camera field of view. Pertinent information may include image size, name, resolution, location, and date. Time could also be saved by coding the programs in C language and running them on a workstation with high speed and large active memory capabilities. A serious effort to improve video measurement techniques is required to convince the scientific community of the measurement capabilities within the video realm. The increased number of unique observation opportunities, alone, may help to increase our understanding of the coastal environment.

APPENDIX A:
LISTING OF EQUIPMENT AND VENDORS

Hardware:

Product	Model	Manufacturer	Address/Phone
Data Loggers	PUV/Turbidity	UF COE	336 Weil Hall, UF Gainesville, FL 32611 904-392-1436
Frame Grabber	DT3851-8	Data Translation	100 Locke Dr. Marlboro, MA 01752 508-481-3700
Hi8 Camera	CCD-V99	Sony	Sony Drive Park Ridge, NJ 07656 201-930-7669
Image Capture Board	Computer Eyes/RT	Digital Vision, Inc.	270 Bridge St. Dedham, MA 02026 617-329-5400
Personal Computer	486DX/50E	Gateway 2000	610 Gateway Dr. N. Sioux City, SD 57049 605-232-2000
Total Station	Omni-1 Model 3006	Alpha Electronics	Littleton, CO 80161 303-795-8435
VHS	AG-1960	Panasonic	50 Meadowland Pkwy. Secaucus, NJ 07094 201-348-7620
Video Monitoring System	VM-2	Erdman Video Systems	2301 Collins Ave, #A336 Miami Beach, FL 33139 305-531-8511

Commercial Software:

Product Description	Manufacturer	Address/Phone
Autocad	Autodesk, Inc.	2320 Marinship Way Sausalito, CA 94965 415-331-8093

DOS 5.0	Microsoft Corp.	1 Microsoft Way Redmond, WA 98052 800-426-9400
Global Lab Image	Data Translation	Marlboro, MA 01752
Image Alchemy 1.7	Handmade Software	15951 Los Gatos Blvd. Suite 17 Los Gatos, CA 95032 800-358-3588
MATLAB 4.0	The Math Works, Inc.	24 Prime Park Way Natick, MA 01760 508-653-1415
Tidemaster	Zephyr Services	1900 Murray Ave. Pittsburgh, PA 15217
Windows 3.1	Microsoft Corp.	Redmond, WA 98052
Word for Windows 2.0c	Microsoft Corp.	Redmond, WA 98052

APPENDIX B:
PROGRAM LISTINGS

```
%%%%%%%%%%%%%%%%%%%%%%%%%%%%%%%%%%%%
% m file to solve transformation equations for oblique image rectification
% solve equations in terms of ground targets for focal length, tilt, phi
% transform and map pixels to new locations
% by Tim Mason  rev. 7/19/93
%%%%%%%%%%%%%%%%%%%%%%%%%%%%%%%%%%%%

% input original coordinates and swing angle (if known), transfer to
% principal plane coordinates

np=input('Enter # of control points ');
x0=zeros(2,1);
x0(1)=input('initial guess focal length [m] ');
x0(2)=input('initial guess camera tilt [radians] ');
zc=input('camera elevation above MSL [m] ');
xf=input('x image control array in column form [fiducial pixels] ');
yf=input('y image control array ');
xgp=input('Cross shore (x) ground control array [m] ');
ygp=input('Long shore (y) ground control array ');
zg=input('z ground control array ');
p=input('initial guess for phi [degrees clockwise from Xg to E] ');

 % input ground/camera coordinate offsets(origin of N-E in X-Y)
 % also change in control.m if used

disp('Enter ground coordinate offsets relative to camera coordinates: ')
xo=input('Xg offset: ');
yo=input('Yg offset: ');

%phi=control(p);              % use if you want to solve for swing angle phi
phi=p*pi/180;

% convert image pixels to screen mm (1 pixel=.325 mm)
% alter as necessary for various monitors


theta=input('enter swing theta [degrees clockwise from vertical]: ');
theta=theta*pi/180;
if theta~=0,
        xf=.000325*(xf.*cos(theta)-yf.*sin(theta));
        yf=.000325*(xf.*sin(theta)+yf.*cos(theta));
else
        xf=xf*.000325;
```

```
        yf=yf*.000325;
end

% convert xgp,ygp to correct coordinate system

disp('initializing...')
xg=xgp*cos(phi)+ygp*sin(phi)+xo;
yg=ygp*cos(phi)-xgp*sin(phi)+yo;

% now solve equations for focal length and tilt by least squares

detail=zeros(16,1);
detail(4,1)=1;
c=zeros(6,np);
for i=1:np,
        c(1,i)=xf(i);
        c(2,i)=yf(i);
        c(3,i)=xg(i);
        c(4,i)=yg(i);
        c(5,i)=zg(i);
        c(6,i)=zc;
end

soln=leastsq('focal',x0,[],[],c,np);
phi
fc=soln(1)
t=soln(2)
disp('hit any key to continue...')
pause
clear xgp ygp x0 zg c p np xf yf xg yg detail soln

a=input('enter image height ');
b=input('enter image width ');
res=input('enter desired output resolution [m/pixel] ');
save inp a b zc fc t phi xo yo res

% Initialize ground and image arrays

        Ng=zeros(1,b);
        Eg=zeros(a,1);
        Xg=zeros(a,b);
        Yg=Xg;

        disp('initializing arrays')
        for j=1:b
                Ng(1,j)=(502-j)*(res);      % res is rectified grid m/pixel
        end
        for i=1:a
                Eg(i,1)=(460-i)*(res);      % (a,b) =location of final grid origin
        end                                  % on rectified map (default = (0,0))
```

```
% transform Eg,Ng axes to Xg,Yg camera axes
disp('Transforming ground coordinates')

        for i=1:a
                for j=1:b
                        Xg(i,j)=Eg(i,1)*cos(phi)+Ng(1,j)*sin(phi)+xo;
                        Yg(i,j)=Ng(1,j)*cos(phi)-Eg(i,1)*sin(phi)+yo;
                end
        end
        clear Eg Ng  res

% save camera/ground grid for use with other similar images
save inp2 Xg Yg

num=input('Enter number of images to rectify')

for s=1:num,
        file(s,:)=input('filename (pad w/ spaces to 5 characters): ','s');
        id(s)=input('# of significant characters in filename: ');
end

for s=1:num,

        disp('loading image')
        nam=file(s,1:id(s));
        eval(['load ' nam '.asc'])
        gi=zeros(a,b);
        gi=eval(nam);
        gg=zeros(a,b);     % initialize ground-rectified grid


%  find (xi,yi) which correspond to (Xg,Yg) and map gi value to gg

        disp('remapping values')
        for i=1:a
                i
                for j=1:b
                        yq=fc*tan(atan(Yg(i,j)/zc)-t);
                        xq=Xg(i,j)*sqrt((yq^2+fc^2)/(zc^2+Yg(i,j)^2));

        %%%%%%%% compensate back for swing angle

                        if theta ~= 0,
                                xq=xq*cos(theta)+yq*sin(theta);
                                yq=yq*cos(theta)-xq*sin(theta);
                        end
                % convert to pixels and round to nearest integer
                        yq=round(yq/3.25e-4);
                        xq=round(xq/3.25e-4);
                        m=(b/2)+xq;
                        k=((a/2)+1)-yq;
                        if(m>=1 & m<=b)&(k>=1 & k<=a),
                                gg(i,j)=gi(k,m);
                        end
```

```
            end
        end

% save image output matrix for display
        disp('saving output image')
        eval(['save ' nam 'out.asc gg /ascii'])
        eval(['save ' nam ' gg'])
        eval(['clear ' nam])
        clear k m gg gi nam
end




%%%%%%%%%%%%%%%%%%%%%%%%%%%%%%%%%%%%
% function focal to specify transformation equations for images
%%%%%%%%%%%%%%%%%%%%%%%%%%%%%%%%%%%%

function y=focal(x0,c,np)

f=x0(1);
t=x0(2);
y=zeros(2,np);

for i=1:np,
        y(1,i)=c(2,i)-f.*tan(atan(c(4,i)/(c(6,i)-c(5,i)))-t);
        y(2,i)=c(1,i)-c(3,i)*sqrt((c(2,i)^2+f.^2)./((c(6,i)-c(5,i))^2+c(4,i)^2));
end

%%%%%%%%%%%%%%%%%%%%%%%%%%%%%%%%%%%%
%  function control to solve azimuth angle phi with least squares
%%%%%%%%%%%%%%%%%%%%%%%%%%%%%%%%%%%%

function y=control(p)
mp=input('enter number of known horizontal ground control points ');
%  p=input('initial guess for phi (degrees clockwise from Xg to E)' );
p=p*pi/180;
xo=11.43;
yo=186.69;
eg=input('East coordinate ground array in column form ');
ng=input('North coordinate ground array in column form ');
Xg=input('Camera X coordinate ground array ');
Yg=input('Camera Y coordinate ground array ');
for i=1:mp
    d(1,i)=Xg(i);
    d(2,i)=Yg(i);
    d(3,i)=eg(i);
    d(4,i)=ng(i);
end
p1=leastsq('angle',p,[],[],xo,mp,d);
p2=leastsq('angl',p,[],[],yo,mp,d);
p3=(p1+p2)/2
```

```
clear mp eg ng Xg Yg i
y=p3;


%%%%%%%%%%%%%%%%%%%%%%%%%%%%%%%%%%%%%%%%%%%%%%
% function angl to specify first equation of ground transformation
%%%%%%%%%%%%%%%%%%%%%%%%%%%%%%%%%%%%%%%%%%%%%%

function y=angl(phi,yo,mp,d)
y=zeros(1,mp);
for i=1:mp
    y(1,i)=d(4,i)*cos(phi)-d(3,i)*sin(phi)+yo-d(2,i);
end


%%%%%%%%%%%%%%%%%%%%%%%%%%%%%%%%%%%%%%%%%%%%%%%%%
% function angle to specify second equation of ground transformation
%%%%%%%%%%%%%%%%%%%%%%%%%%%%%%%%%%%%%%%%%%%%%%%%%

function y=angle(phi,xo,mp,d)
y=zeros(1,mp);
for i=1:mp
    y(1,i)=d(3,i)*cos(phi)+d(4,i)*sin(phi)+xo-d(1,i);
end
```

REFERENCES

Aagaard, T. and J. Holm, 1989. "Digitization of Wave Run-Up Using Video Records." *J. Coastal Res.*, 5(3): 547-551.

Coastal Planning & Engineering, 1992. "Hollywood/Hallandale First Periodic Beach Renourishment Project 6 Month Follow-Up Study." Boca Raton, FL.

Dompe, P.E., 1993. "Natural Fluctuations in Nearshore Turbidity and the Relative Influences of Beach Renourishment." UFL/COEL-93/004, Coastal and Ocean. Eng. Dept., University of Florida, Gainesville, FL.

Dompe, P.E. and D.M. Hanes, 1992. "Wave Data Summary: Holloywood Beach, Florida, January 1990 to May 1992." UFL/COEL-92/016, Coastal and Ocean. Eng. Dept., University of Florida, Gainesville, FL.

Fredsoe, J. and R. Deigaard, 1992. *Mechanics of Coastal Sediment Transport,* World Scientific, Singapore.

Gonzalez, R.C. and P. Wintz, 1987. *Digital Image Processing*, 2nd Edition, Addison-Wesley, Reading, MA.

Goodwin, C.R. and D.M. Michaelis, 1984. "Appearance and Water Quality of Turbidity Plumes Produced by Dredging in Tampa Bay, Florida." US Geological Survey Water-Supply Paper 2192, 66 p.

Holland, K.T., R.A. Holman, and A.H. Sallenger, 1991. "Estimation of Overwash Bore Velocities Using Video Techniques." *Coastal Sediments '91 Proc.*, ASCE, New York: 489-497.

Holman, R.A. and R.T. Guza, 1984. "Measuring Run-Up on a Natural Beach." *Coastal Engineering,* 84(8): 129-140.

Holman, R., P. Howd, J. Oltman-Shay, and P. Komar, 1990. "Observations of the Swash Expression of Far Infragravity Wave Motions." *Proc. 22nd Conference on Coastal Engineering,* ASCE, New York: 1242-1253.

Holman, R.A. and T.C. Lippmann, 1987. "Remote Sensing of Nearshore Bar Systems - Making Morphology Visible." *Coastal Sediments '87,* ASCE, New York: 929-944.

Holman, R.A. and T.C. Lippmann, 1989. "Wave Dissipation on a Barred Beach: A Method for Determining Sand Bar Morphology," CERC Final Report, US Army Engineer Watereays Experiment Station, Vicksburg, MS.

Holman, R.A., T.C. Lippmann, P.V. O'Neill, and K. Hathaway, 1991. "Video Estimation of Subaerial Beach Profiles." *Marine Geology*, 97: 225-231, Elsevier Science Publishers, Amsterdam.

Lillesand, T.M. and R.W. Kiefer, 1987. *Remote Sensing and Image Interpretation,* 2nd Edition, John Wiley and Sons, New York.

Lippmann, T.C. and R.A. Holman, 1989. "Quantification of Sand Bar Morphology: A Video Technique Based on Wave Dissipation." *J. Geophys. Res.*, 94(C1): 995-1011.

Lippmann, T.C. and R.A. Holman, 1991. "Phase Speed and Angle of Breaking Waves Measured With Video Techniques." *Coastal Sediments '91 Proc.*, ASCE, New York: 542-556.

Loomer, S.A. and P.R. Wolf, 1974. "Terrestrial Photogrammetric Measurements of Surface Water Velocities." Universty of Wisconsin Sea Grant College Reprint WIS-SG-74-352.

Maresca, J.W., Jr. and E. Seibel, 1976. "Terrestrial Photogrammetric Measurements of Breaking Waves and Longshore Currents in the Nearshore Zone." *Proc. 15th Conference on Coastal Engineering,* ASCE, New York: 681-700.

Wolf, P.R., 1983. *Elements of Photogrammetry*, 2nd Edition, McGraw-Hill, New York.

BIOGRAPHICAL SKETCH

The author was brought into this world on September 28, 1968, in a suburban town in Bucks County, Pennsylvania. Each summer, time was spent in the Huntington Beach of New Jersey, Ocean City, where he discovered his love for the ocean and the sports of surfing and skimboarding. While landlocked throughout the colder months, the author developed his musical skills by playing drums and percussion in academically based groups and a somewhat locally notorious rock band.

Upon high school graduation he decided to forego the pursuit of a career as a professional drummer and enrolled in the ocean engineering program at Florida Atlantic University. Time apart from his studies was spent travelling to Puerto Rico, California, Costa Rica, and the Bahamas for surfing. He continued with the drums in several bands and expanded to the guitar in the absence of drums.

After graduating with honors, he attended graduate school at the University of Florida Department of Coastal and Oceanographic Engineering. Future plans include employment with Applied Technology and Management,a consulting firm which works on sound solutions to the problems that are plaguing our coastal environment.